JEM Journal of Experimental Medicine

ARTICLE

Neutrophils facilitate ovarian cancer premetastatic niche formation in the omentum

WonJae Lee[1], Song Yi Ko[1], Muhaned S. Mohamed[1], Hilary A. Kenny[2], Ernst Lengyel[2], and Honami Naora[1]

Ovarian cancer preferentially metastasizes to the omentum, a fatty tissue characterized by immune structures called milky spots, but the cellular dynamics that direct this tropism are unknown. Here, we identified that neutrophil influx into the omentum is a prerequisite premetastatic step in orthotopic ovarian cancer models. Ovarian tumor–derived inflammatory factors stimulated neutrophils to mobilize and extrude chromatin webs called neutrophil extracellular traps (NETs). NETs were detected in the omentum of ovarian tumor–bearing mice before metastasis and of women with early-stage ovarian cancer. NETs, in turn, bound ovarian cancer cells and promoted metastasis. Omental metastasis was decreased in mice with neutrophil-specific deficiency of peptidylarginine deiminase 4 (PAD4), an enzyme that is essential for NET formation. Blockade of NET formation using a PAD4 pharmacologic inhibitor also decreased omental colonization. Our findings implicate NET formation in rendering the premetastatic omental niche conducive for implantation of ovarian cancer cells and raise the possibility that blockade of NET formation prevents omental metastasis.

Introduction

A widely recognized feature of epithelial ovarian cancer, the fifth leading cause of cancer death in women, is i.p. seeding (Tan et al., 2006; Lengyel, 2010; Sodek et al., 2012). This form of dissemination has been described as a passive process in which cancer cells shed from tumors, are circulated by the mechanical flow of peritoneal fluid, and then implant on peritoneal surfaces (Tan et al., 2006; Lengyel, 2010; Sodek et al., 2012). 60% of women who are diagnosed with ovarian cancer present with advanced-stage, disseminated disease, and in almost all advanced-stage cases, the omentum is colonized (Lengyel, 2010). The omentum is an apron-like structure that drapes from the stomach and is composed of fat and connective tissues lined by mesothelial cells (Meza-Perez and Randall, 2017). Growth of ovarian tumor implants on the omentum is stimulated by lipids derived from omental adipocytes and by cytokines that are secreted by omental fibroblasts and adipose mesenchymal stem cells (Nieman et al., 2011; Ko et al., 2012). However, the mechanisms that cause circulating ovarian cancer cells to preferentially home to, and implant on, the omentum are poorly understood. Previous studies have identified that implantation of ovarian cancer cells is facilitated by several cell surface molecules, such as CD44, P-cadherin, and α5β1 integrin, that promote the interaction of cancer cells with mesothelial cells or with the submesothelial extracellular matrix (Strobel et al., 1997; Iwanicki et al., 2011; Usui et al., 2014). However, all visceral surfaces are lined by mesothelial cells, and thus interactions with mesothelial cells might not solely account for the tropism of ovarian cancer cells for the omentum.

The omentum was described over 100 years ago as "the policeman of the abdomen" and has been long recognized to play essential functions in peritoneal defense (Meza-Perez and Randall, 2017). A hallmark of the omentum, which distinguishes this tissue from other visceral fat pads, is its abundance of highly vascularized immune cell structures called milky spots (Hagiwara et al., 1993). Milky spots are mainly composed of lymphocytes and macrophages and are preferentially colonized by cancer cells (Hagiwara et al., 1993; Meza-Perez and Randall, 2017). Intriguingly, it has been observed that ovarian cancer cells colonize the omentum of mice with deficiencies in T, B, and/or natural killer cells as effectively as in immunocompetent mice (Clark et al., 2013). These findings strongly implicate nonlymphoid immune cell constituents in the predilection of ovarian cancer cells for the omentum. Macrophages secrete cytokines that stimulate ovarian tumor angiogenesis and immune evasion (Robinson-Smith et al., 2007; Ko et al., 2014), and a recent study has shown that the density of macrophages in the omentum increases concomitantly with the extent of disease at this site (Pearce et al., 2018). However, macrophages might not fully explain the propensity of ovarian cancer cells to home to the omentum as macrophages

[1]Department of Molecular and Cellular Oncology, University of Texas MD Anderson Cancer Center, Houston, TX; [2]Section of Gynecologic Oncology, Department of Obstetrics and Gynecology, University of Chicago, Chicago, IL.

Correspondence to Honami Naora: hnaora@mdanderson.org.

comprise almost 60% of the cellular content of peritoneal fluid and are abundant at multiple sites throughout the peritoneal cavity (van Furth et al., 1979).

Bone marrow–derived neutrophils act as the first line of defense in response to pathogens or tissue damage and are normally present at low abundance in the omentum and in peritoneal fluid (<1% of cellular content; Fruhman, 1960; Cohen et al., 2013). Recently, it was reported that neutrophils, in response to peritoneal infection or injury, principally mobilize into the abdominal cavity through specialized vessels called high endothelial venules (HEVs) in omental milky spots (Buscher et al., 2016). We therefore hypothesized that the establishment of the premetastatic omental niche in ovarian cancer involves the influx of neutrophils at this site. In this study, we identified that recruitment of neutrophils to the omentum is an essential step that precedes the colonization of this site by ovarian cancer cells. Furthermore, we identified that early-stage ovarian tumors induce omental neutrophils to extrude chromatin fibers and that blockade of this neutrophil response inhibits entrapment of circulating ovarian cancer cells in the omental niche.

Results

Neutrophils accumulate in the premetastatic omental niche

To initiate this study, we evaluated metastatic tropism of ovarian cancer in an immunocompetent syngeneic orthotopic model. The ID8 cell line is the most widely used mouse ovarian cancer line and forms tumors that mimic the typical behavior of human ovarian cancer (Roby et al., 2000). We used ID8 cells that stably express luciferase and GFP to detect tumors in mice by bioluminescence imaging and to quantify tumor cells in tissues by flow cytometry. Orthotopic tumors were generated by injecting ID8 cells intrabursally (i.b.) into immunocompetent C57BL/6 mice. These tumors predominantly metastasized to the omentum (Fig. 1, A and B). ID8 cells also preferentially formed implants on the omentum following i.p. injection into either immunocompetent or NOD-*scid* IL2Rγ^{null} (NSG) mice (Fig. 1, A and B). Furthermore, cells of the human ovarian cancer cell line ES2 showed tropism for the omentum in nude mice (Fig. 1, A and B). To more closely evaluate the omentum, mouse omental tissues were stained for CD31 to visualize total vasculature and for peripheral node addressin (PNAd) to visualize HEVs in milky spots as performed in a recent study (Buscher et al., 2016; Fig. 1 C). At the earliest stage of dissemination, ovarian cancer cells were predominantly detected adjacent or close to PNAd$^+$ vessels in omental milky spots and were rarely found in surrounding tracts of adipocytes (Fig. 1 D). Similar observations were found in clinical specimens of omental tissues of women with ovarian cancer (Fig. 1, E and F). These findings indicate that ovarian cancer cells preferentially implant on the omentum and particularly within milky spots. Furthermore, this metastatic tropism for the omentum occurs irrespective of orthotopic or i.p. engraftment and is not affected by lymphoid deficiency consistent with an earlier study (Clark et al., 2013).

We next evaluated the kinetics of ovarian cancer cell implantation and determined the abundance of the major myeloid cell types in the omentum at several time points before colonization of this site. At 3 wk following i.b. injection of ID8 cells into C57BL/6 mice, primary tumors had become established and were palpable (Fig. S1, A and B). Metastasis became palpable in the omentum at 4 wk but was not detected at 3 wk (Fig. S1 C). At 1 wk and 2 wk, the abundance of neutrophils in the omentum did not significantly change (Fig. 2 A). However, at 3 wk, when primary tumors had become established, the abundance of neutrophils in the omentum of these mice significantly increased and was approximately sevenfold higher than that of saline-injected control siblings ($P < 0.01$; Fig. 2 A). In contrast, the abundance of macrophages in the omentum did not significantly increase during the premetastatic stage (Fig. 2 B). Neutrophils were mostly localized close to PNAd$^+$ vessels in the omentum during the premetastatic stage (Fig. 2 C), suggesting that the increased abundance occurs through influx via HEVs. We also evaluated nude mice following i.p. injection of ES2 cells. In this model, cancer cell implantation was first detected in the omentum at day 5 (Fig. S1 D). Neutrophil abundance in the omentum did not significantly change at day 1 but at day 4 had increased approximately sixfold and without a significant change in macrophage abundance (Fig. S2, A–C). In contrast to the omentum, other peritoneal fat tissues (perirenal, gonadal, and mesenteric) showed no significant increases or only modest increases (i.e., less than twofold) in neutrophil abundance before colonization in orthotopic models (Fig. 2 A) and in i.p. models (Fig. S2 B). Furthermore, numbers of circulating neutrophils did not significantly increase in mice with orthotopic tumors during the premetastatic stage (Fig. 2 D). A modest but statistically significant increase in circulating neutrophils (i.e., 1.7-fold, $P < 0.001$) was observed just before colonization in i.p. models (Fig. S2 D). Circulating Ly6G$^+$ cells in these mice exhibited multilobulated segmented morphology that is characteristic of neutrophils and was similar that of non–tumor-bearing mice (Fig. S2 E). Polymorphonuclear myeloid-derived suppressor cells (PMN-MDSCs) also express Ly6G but, in contrast to neutrophils, have been reported to additionally express CD115 or CD244 (Youn et al., 2012). CD115 and CD244 were detected in only ∼1% of Ly6G$^+$ cells in mice with early-stage tumors (Fig. S2 F), suggesting that the majority of these cells are neutrophils. Collectively, these findings indicate that the abundance of neutrophils increases in the omentum before colonization of this site by ovarian cancer cells.

To confirm our findings from mouse studies, we evaluated clinical specimens of omental tissues of women with a confirmed diagnosis of International Federation of Gynecology and Obstetrics (FIGO) stage I or II high-grade serous carcinoma (HGSC; i.e., disease that is ovarian-confined or locally extended to adjacent pelvic structures). Significantly higher numbers of cells that were positive for neutrophil elastase, a protease that is predominantly found in granules of neutrophils (Kramps et al., 1984), were detected in omental tissues of women with early-stage HGSC than in normal omental tissues of women without cancer ($P < 0.01$; Fig. 2 E). Notably, cells that are positive for neutrophil elastase and that have multilobulated segmented morphology were prominently detected in abundance around vessels in omental tissues of women with early-stage HGSC (Fig. 2, F and G). These findings strongly support the notion that neutrophil influx is a feature of the premetastatic omental niche.

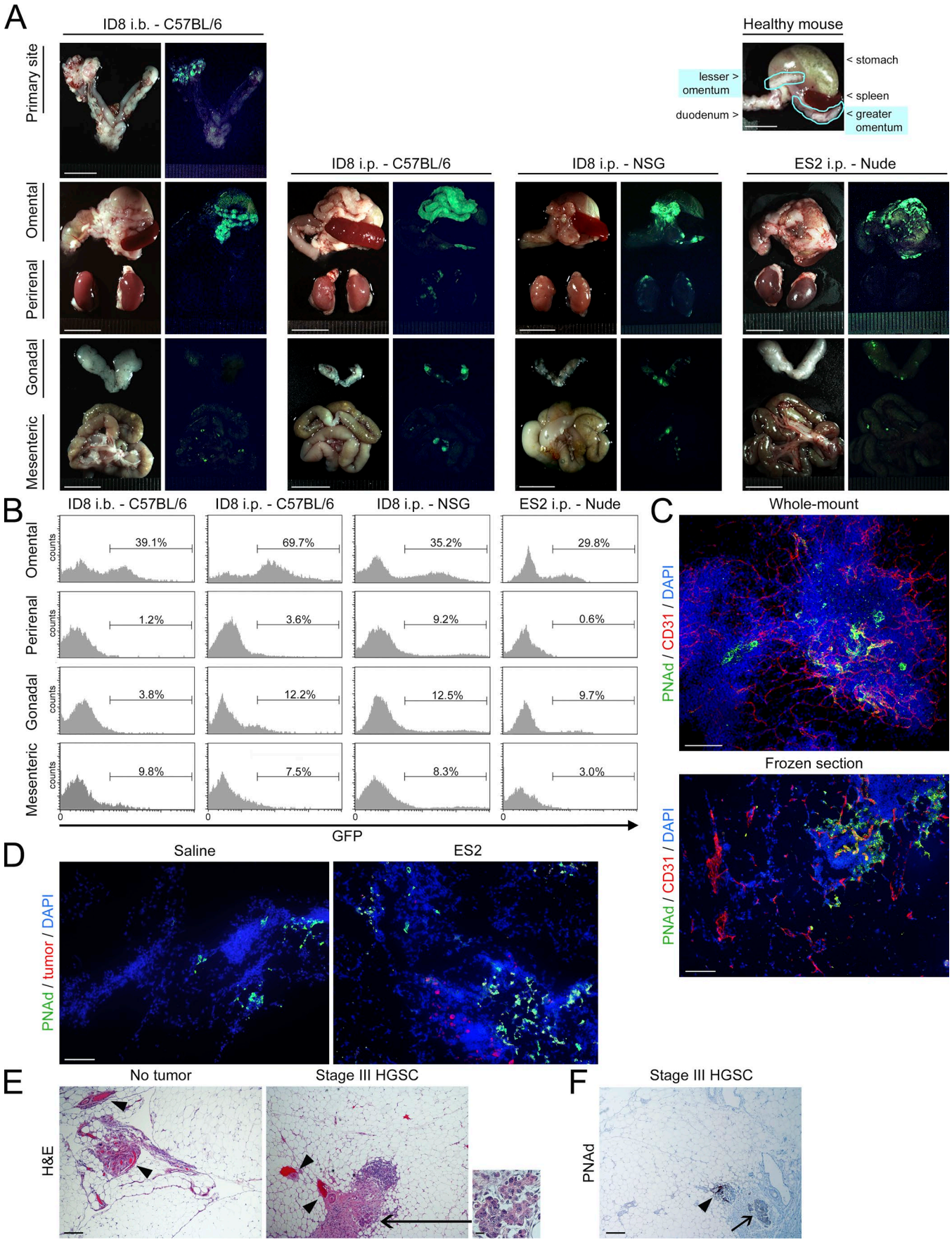

Neutrophils facilitate ovarian cancer cell implantation on the omentum

Because we observed a striking increase in neutrophil abundance in the omentum before palpable colonization of this site, we investigated whether depletion of neutrophils decreases the formation of omental tumor implants. Immunocompetent mice were injected i.b. with ID8 cells and at 3 wk thereafter confirmed for primary tumor formation by bioluminescence imaging. Mice were then randomized into groups that were treated for 3 wk either with antibody (Ab) to Ly6G to deplete neutrophils or with control Ig (Fig. 3 A). Efficacy of neutrophil depletion by Ly6G Ab was confirmed by flow cytometric analysis (Fig. 3 B) and by complete blood count (CBC) test ($P < 0.0001$ for neutrophils and not significant for other blood cells; Fig. 3 C). Sizes of tumors were determined from luminescence signals (Fig. 3, D and E). In addition, the abundance of GFP^+ tumor cells in individual tissues was quantified (Fig. 3, F and G). Depletion of neutrophils by Ly6G Ab did not significantly reduce the size of primary tumors (Fig. 3, D–G). However, mice that were treated with Ly6G Ab developed significantly less omental metastasis than control mice (i.e., ∼70% reduction, $P < 0.01$; Fig. 3, D–G). Depletion of neutrophils by Ly6G Ab also significantly inhibited cancer cell implantation on the omentum of nude mice following i.p. injection of ES2 cells ($P < 0.01$; Fig. S2, G–I). These findings indicate that neutrophils facilitate the formation of ovarian tumor implants on the omentum.

Ovarian cancer cell–derived factors induce neutrophils to mobilize and to extrude chromatin

We subsequently investigated the reciprocal effect of ovarian cancer cells on neutrophils. Stimulation of normal human peripheral blood neutrophils with media conditioned by ES2 cells induced neutrophil chemotaxis within 2 h (Fig. S3 A). By 4 h, neutrophils were observed to extrude webs of DNA that were detected by staining with Sytox Green, a cell-impermeable DNA dye (Fig. 4 A, top). Neutrophils undergo a unique form of caspase-independent cell death called NETosis in which chromatin fibers called neutrophil extracellular traps (NETs) are extruded (Brinkmann et al., 2004; Fuchs et al., 2007). A hallmark of NETosis is citrullination of histones that causes chromatin to decondense and extrude (Wang et al., 2009). Citrullinated histone H3 (cit-H3) was detected in DNA extruded by human neutrophils following stimulation with ES2-conditioned media (Fig. 4 A, bottom). Identical results were obtained when normal mouse bone marrow neutrophils were stimulated with media conditioned by ID8 cells (Fig. 4 B). As a positive control, we stimulated neutrophils with PMA, a potent inducer of NETosis (Fuchs et al., 2007; Fig. 4, A and B). These findings indicate that ovarian cancer cell–derived factors stimulate neutrophil chemotaxis and also induce NET formation.

Several neutrophil chemotactic factors have been detected at elevated levels in body fluids of women with ovarian cancer, including IL-8, monocyte chemoattractant protein-1 (MCP-1), growth-regulated oncogene–α and –β (GROα and GROβ), and G-CSF (Negus et al., 1995; Gorelik et al., 2005; Taki et al., 2018). IL-8, MCP-1, GROα, and GROβ were detected in ovarian cancer cell–conditioned media by screening with a cytokine Ab array, and levels of these factors were confirmed by ELISA (Fig. S3, B and C). G-CSF was not detected on the array, but its presence in conditioned media was confirmed by ELISA (Fig. S3 C). As expected, chemotaxis of neutrophils was reduced following stimulation with conditioned media that had been depleted of any one of those five cytokines (Fig. S3, A and C). NET formation was decreased by depletion of IL-8, G-CSF, GROα, or GROβ, but not of MCP-1 (Fig. S3 D). These findings indicate that several, though not all, ovarian cancer cell–derived factors that stimulate neutrophil chemotaxis can also stimulate NETosis.

Early-stage ovarian cancers induce NET formation in the premetastatic omental niche

Because the premetastatic omental niche is characterized by neutrophil influx and ovarian cancer cells secrete factors that induce neutrophils to form NETs, we investigated the possibility that early-stage ovarian tumors induce NET formation in the omentum. Immunocompetent mice were injected i.b. with ID8 cells and at 3 wk thereafter confirmed for primary tumor formation and lack of palpable metastasis. Control mice were injected i.b. with saline. Because microbes can induce NET formation (Brinkmann et al., 2004), both groups of mice were administered antibiotic before and following i.b. injection. Omental tissues were then stained with Ly6G Ab and with Sytox Red dye to detect extruded DNA, and staining was evaluated by flow cytometry. The proportion of omental $Ly6G^+$ cells that extruded DNA was significantly higher in mice with primary tumors than in saline-injected control mice ($P < 0.01$; Fig. 5 A). $Ly6G^+$ cells that were positive for cit-H3 were prominently detected in omental tissues of C57BL/6 mice

Figure 1. **Ovarian cancer cells preferentially implant on the omentum, and this tropism is not affected by lymphoid deficiency. (A and B)** GFP-expressing ID8 cells were injected i.b., between the left ovary and oviduct and contralateral to the omentum, into immunocompetent C57BL/6 mice, and tumors were evaluated at 6 wk thereafter. ID8 cells were injected i.p. into female immunocompetent C57BL/6 and NSG mice, and tumors were evaluated at 10 wk thereafter. GFP-expressing ES2 cells were injected i.p. into female nude mice, and tumors were evaluated at 9 d thereafter. Five mice per group were evaluated. **(A)** Representative images of tissues in each group viewed under light and fluorescence microscopy. Location of the omentum in a healthy mouse is also shown. Bars, 10 mm. **(B)** Representative flow cytometric analyses of the abundance of GFP^+ tumor cells in each visceral fat tissue (omental, perirenal, gonadal, and mesenteric), expressed as a percentage of the nonfat cellular content in each tissue. **(C)** Visualization of total vasculature ($CD31^+$; red) and HEVs in milky spots ($PNAd^+$; green) in the naive mouse omentum by immunofluorescence staining of whole mount (top) and frozen (bottom) sections. Bars, 100 µm. Shown are representative results of three independent experiments. **(D)** Omental tissues were collected from nude mice at 5 d following i.p. injection of ES2 cells or saline ($n = 5$ mice per group). Frozen sections were stained to detect cancer cells (red) and $PNAd^+$ vessels in milky spots (green). Bar, 100 µm. Shown are representative examples of staining. **(E and F)** Omental tissues of women without cancer and with stage III HGSC were stained with (E) H&E and with (F) Ab to PNAd ($n = 3$ cases per group). Bar, 200 µm. Indicated are vessels within or adjacent to milky spots (arrowheads) and tumor foci (arrows). Inset shows foci at higher magnification. Bar, 20 µm. Shown are representative examples of staining.

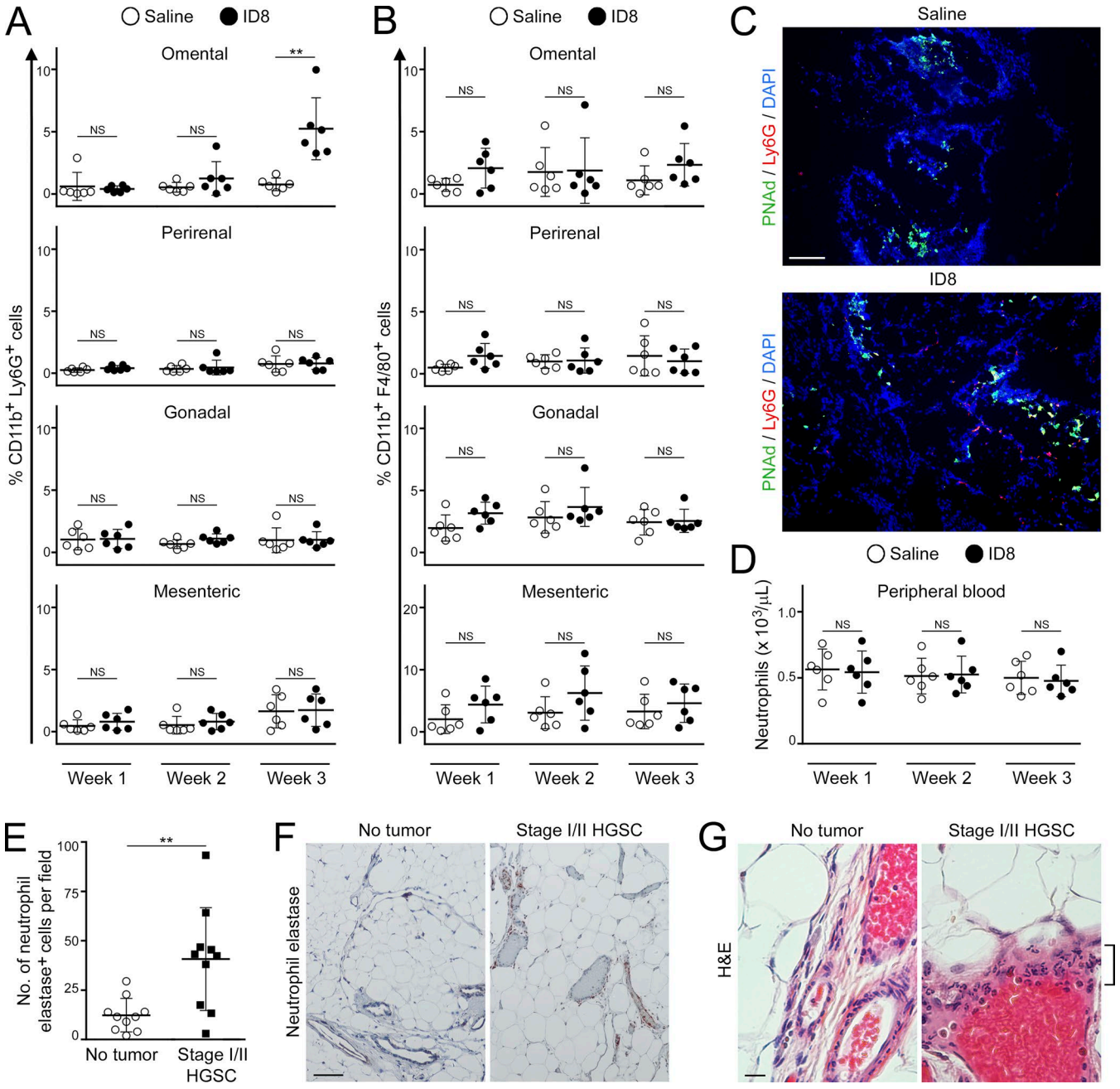

Figure 2. **Early-stage ovarian tumors trigger an increase in neutrophil abundance in the premetastatic omental niche. (A and B)** Immunocompetent C57BL/6 mice were injected i.b. with ID8 cells that express GFP and luciferase. Control siblings were injected i.b. with saline. Mice were evaluated at 1, 2, and 3 wk thereafter (n = 6 mice per group at each time point). Absence of palpable metastasis was confirmed in the ID8 groups by bioluminescence imaging and by flow cytometric analysis of tissues ex vivo. Visceral fat tissues of each mouse in the ID8 and control groups were stained with Abs to CD11b, Ly6G, and F4/80, and staining was analyzed by flow cytometry. Shown are the abundance of $CD11b^+Ly6G^+$ cells (neutrophils; A) and $CD11b^+F4/80^+$ cells (macrophages; B), expressed as percentages of the nonfat cellular content in each tissue. **, $P < 0.01$ (unpaired t test). **(C)** Staining of $Ly6G^+$ cells (red) and $PNAd^+$ vessels (green) in omental tissues collected from C57BL/6 mice at 3 wk following i.b. injection of nonfluorescent ID8 cells or saline (n = 5 mice per group). Bar, 100 µm. Shown are representative examples of staining. **(D)** Circulating neutrophil counts in C57BL/6 mice were determined by CBC test at 1, 2, and 3 wk following i.b. injection of ID8 cells or saline (n = 6 mice per group at each time point; unpaired t test). **(E–G)** Analysis of omental tissues of women with stage I/II HGSC and without cancer (n = 10 cases per group). **(E)** Average number of neutrophil $elastase^+$ cells for each case in each group. For each case, the average number of neutrophil $elastase^+$ cells was calculated by scoring four random ×100 microscopic fields in stained sections. **, $P < 0.01$ (Mann–Whitney U test). **(F)** Representative examples of neutrophil elastase staining. Bar, 100 µm. **(G)** H&E-stained sections. Cells with segmented morphology characteristic of neutrophils (bracket) are seen surrounding a vessel in omental tissue of a woman with HGSC. Bar, 20 µm. Error bars in A, B, D, and E represent SD.

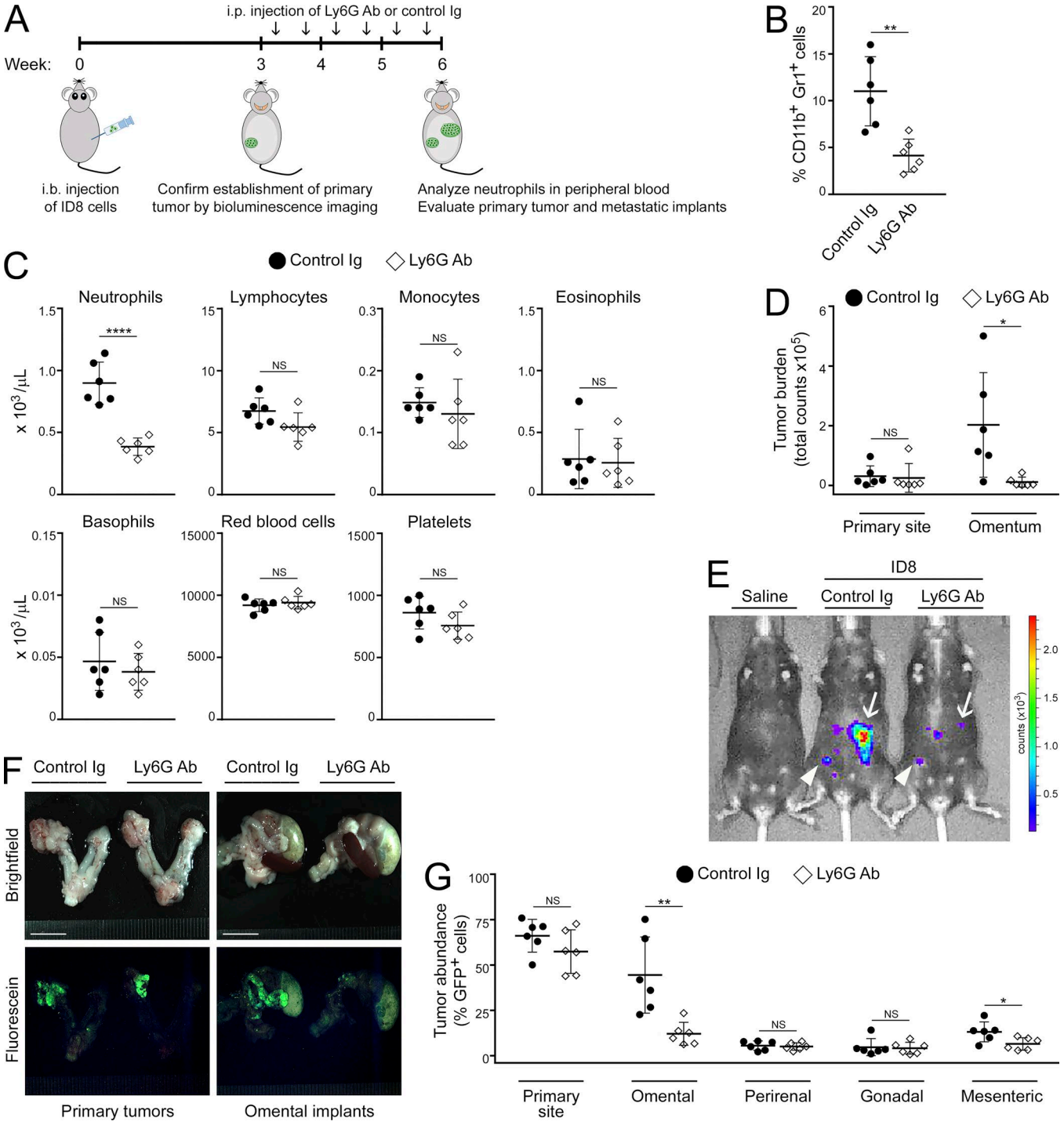

Figure 3. **Neutrophil depletion decreases omental metastasis.** Immunocompetent C57BL/6 mice were injected i.b. with ID8 cells that express GFP and luciferase. At 3 wk thereafter, formation of primary tumors was confirmed by bioluminescence imaging. Mice were then randomized into groups that were administered either Ly6G Ab or control Ig twice a week for 3 wk (n = 6 mice per group). Following Ab treatment, peripheral blood and tumors in each mouse of each group were analyzed. **(A)** Experimental scheme. **(B)** Abundance of neutrophils in peripheral blood, quantified by flow cytometric analysis. **, P < 0.01 (unpaired t test). **(C)** Analysis of peripheral blood by CBC test. ****, P < 0.0001 (unpaired t test). **(D)** Sizes of primary tumors and omental implants detected by bioluminescence imaging and calculated from emitted signals. *, P < 0.05 (unpaired t test). **(E)** Representative images of mice with primary tumors (arrowheads) and omental implants (arrows) detected by bioluminescence imaging. **(F)** Representative images of tissues viewed under light and fluorescence microscopy. Bars, 10 mm. **(G)** Abundance of tumor in tissues of the primary site (left ovary and oviduct) and in visceral fat tissues, quantified by flow cytometric analysis of GFP+ cells. *, P < 0.05; **, P < 0.01 (unpaired t test). Error bars in B–D and G represent SD.

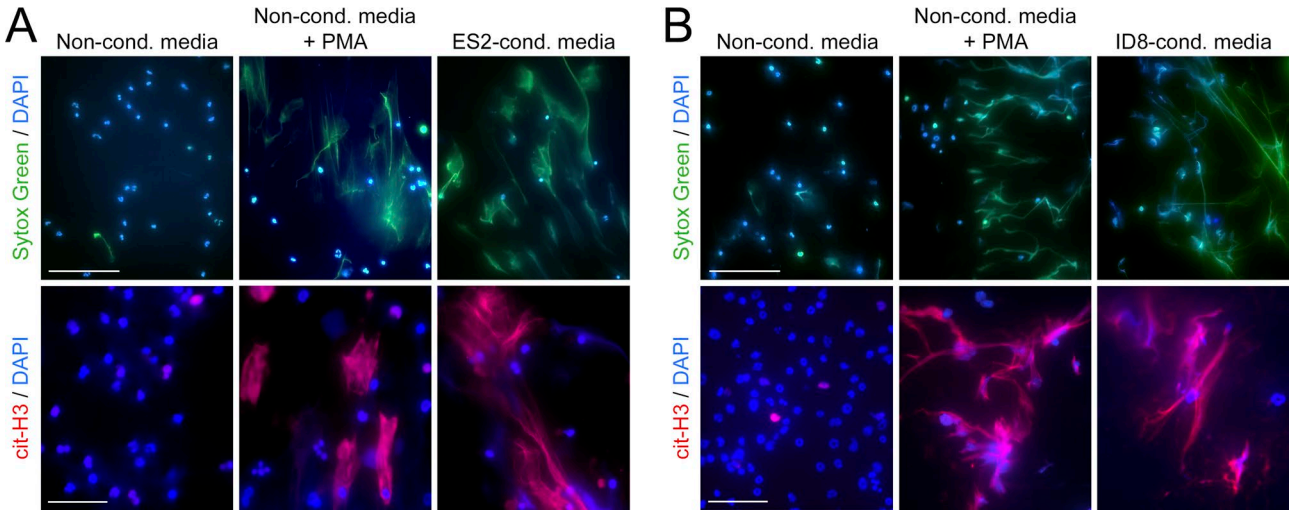

Figure 4. **Ovarian cancer cell–derived factors induce neutrophils to form NETs.** Normal neutrophils were stimulated for 4 h with media conditioned by ovarian cancer cells or with nonconditioned media, without or with the addition of PMA. Thereafter, neutrophils were stained with Sytox Green dye to detect extruded DNA (green) and with cit-H3 Ab (red). Nuclei were visualized by staining with DAPI (blue). Bars, 100 µm (top) and 50 µm (bottom). **(A)** Neutrophils were isolated from peripheral blood of healthy adult donors. Media conditioned by ES2 cells were used. **(B)** Neutrophils were isolated from bone marrow of healthy adult C57BL/6 mice. Media conditioned by ID8 cells were used. In A and B, three independent experiments were performed, with neutrophils from a different donor used in each experiment. Shown are representative images.

with primary orthotopic tumors but were rarely seen in non–tumor-bearing mice (Fig. 5 B). Similar results were obtained in nude mice following i.p. injection with ES2 cells (Fig. S3, E and F).

To confirm our findings from mouse studies, we evaluated NET formation in clinical specimens of formalin-fixed, paraffin-embedded (FFPE) omental tissues of women with stage I or II ovarian cancer. To keep pathological parameters consistent, we analyzed cases with serous histology, the most common ovarian cancer histotype. Omental tissues of women with stage I/II HGSC and with stage I/II serous low malignant potential (SLMP) tumor were evaluated. In contrast to HGSC, SLMP tumors mostly have an indolent clinical course, with ∼75% of SLMP cases diagnosed at stage I/II (Sherman et al., 2004). As a control group, normal omental tissues of women without cancer history were evaluated. Because Sytox dyes are not suitable for staining FFPE tissues, dual immunofluorescence staining of cit-H3 and myeloperoxidase (MPO) was performed to detect NET-positive neutrophils. MPO is required for NETosis and is abundant in NET-positive neutrophils (Metzler et al., 2011). Numbers of $MPO^+cit\text{-}H3^+$ cells in the omentum were significantly higher in women with stage I/II SLMP than in cancer-free women ($P < 0.001$) and higher in women with stage I/II HGSC than in those with SLMP ($P < 0.01$; Fig. 5, C and D). These findings indicate that early-stage ovarian tumors, especially those of high metastatic potential, induce NET formation in the premetastatic omental niche.

Ovarian cancer cells attach to NETs

NETs were originally identified in infectious diseases and found to trap microbes (Brinkmann et al., 2004). To test whether NETs bind ovarian cancer cells, we stimulated mouse neutrophils with ID8-conditioned media or with PMA to induce NETs and then seeded ID8 cells onto neutrophils. A significantly higher number of ID8 cells attached to NET-positive neutrophils than to non-induced neutrophils ($P < 0.01$; Fig. 6, A and B). Identical results were obtained using human ovarian cancer cells and human neutrophils (Fig. 6 C). Furthermore, ovarian cancer cells were predominantly detected in close proximity to $cit\text{-}H3^+$ cells in the mouse omentum (Fig. 6 D). To further investigate the interaction of ovarian cancer cells with NETs, we evaluated neutrophils of mice that are deficient in peptidylarginine deiminase 4 (PAD4). This enzyme is highly expressed in neutrophils and is essential for NET formation (Li et al., 2010). PAD4 converts methyl-arginine residues in histone tails into citrulline, which in turn causes chromatin to decondense and extrude (Wang et al., 2009). Conventional *Padi4*-knockout mice do not form NETs (Li et al., 2010). We generated a conditional knockout model by crossing $Padi4^{fl/fl}$ mice (Hemmers et al., 2011) with MRP8-Cre-ires/GFP transgenic mice in which Cre is expressed in the majority of neutrophils (Passegué et al., 2004; Abram et al., 2014). Neutrophil-specific *Padi4* deficiency in resultant progeny was confirmed by quantitative RT-PCR (qRT-PCR; Fig. S4 A). Neutrophil-specific $Padi4^{-/-}$ mice had normal neutrophil and other blood cell counts, and the gross morphology of neutrophils in these mice was normal (Fig. S4, B and C). The chemotactic response of neutrophils of neutrophil-specific $Padi4^{-/-}$ mice to ovarian cancer cell–conditioned media was not significantly different from that of neutrophils of $Padi4^{+/+}$ mice (Fig. S4 D). However, in contrast to neutrophils of $Padi4^{+/+}$ mice, neutrophils of neutrophil-specific $Padi4^{-/-}$ mice did not form NETs (Fig. 6 E). Whereas stimulation of neutrophils of $Padi4^{+/+}$ mice with cancer cell–conditioned media significantly increased attachment of cancer cells ($P < 0.01$), increased cancer cell attachment was not observed to stimulated neutrophils of neutrophil-specific $Padi4^{-/-}$ mice (Fig. 6 F). Together, these findings indicate that ovarian cancer cells preferentially bind to NET-positive neutrophils and raise the possibility that the NET-rich omental niche traps ovarian cancer cells.

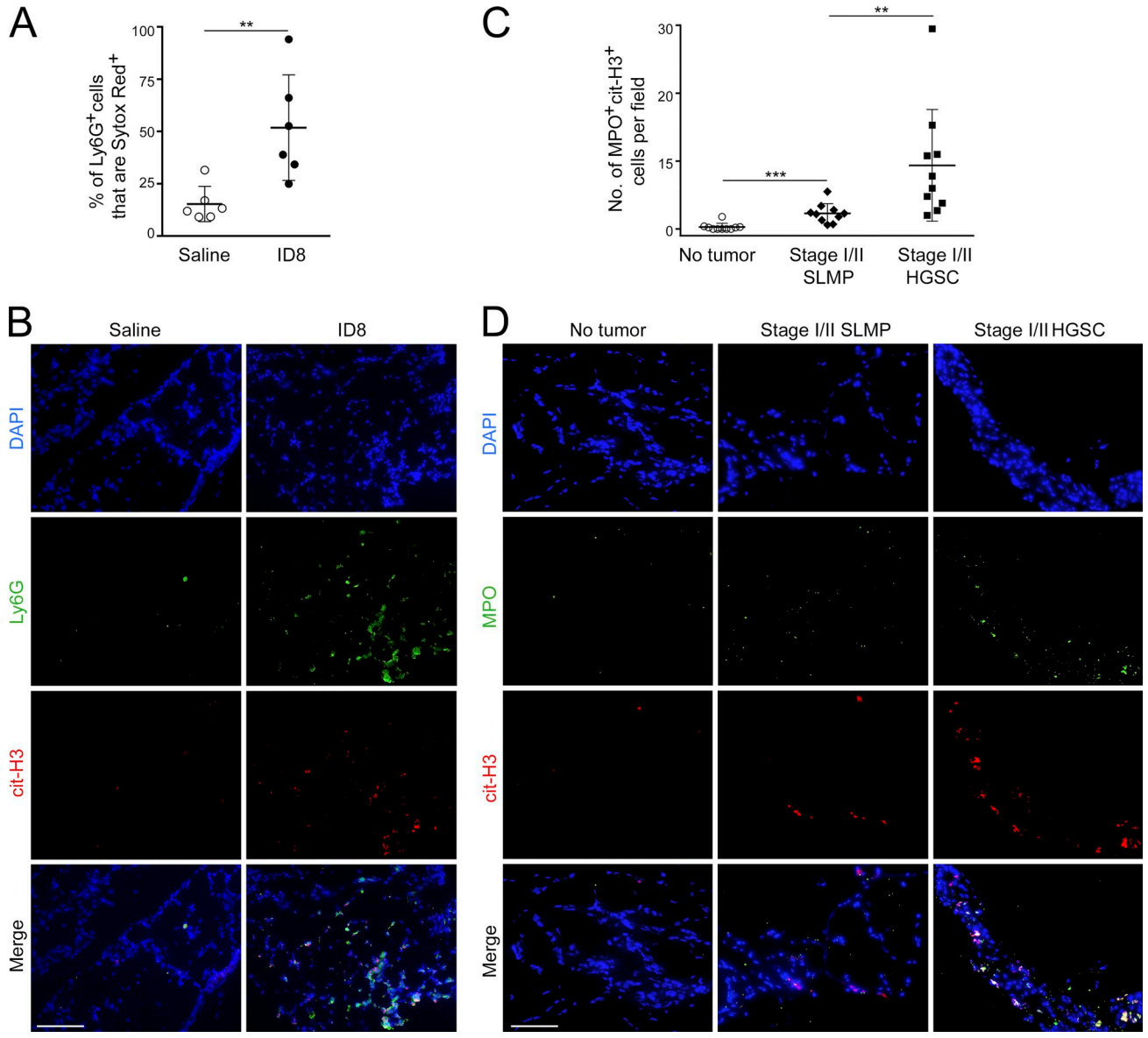

Figure 5. **Early-stage ovarian tumors induce NET formation in the premetastatic omental niche. (A and B)** Analysis of mouse omental tissues. **(A)** C57BL/6 mice were injected i.b. with ID8 cells or with saline (n = 6 mice per group) and euthanized at 3 wk thereafter. Fresh omental tissues were stained with Sytox Red dye to detect extruded DNA and with Ly6G Ab, and staining was analyzed by flow cytometry. Shown are proportions of omental Ly6G$^+$ cells that were Sytox Red$^+$ in each mouse of each group. **, P < 0.01 (unpaired t test). **(B)** Frozen sections of omental tissues were stained to detect Ly6G (green) and cit-H3 (red). Bar, 100 µm. Nonfluorescent ID8 cells were used to inject mice. Shown are representative examples of staining. **(C and D)** Analysis of human omental tissues. Immunofluorescence staining of MPO (green) and cit-H3 (red) was performed on FFPE sections of omental tissues of women with stage I/II HGSC, with stage I/II SLMP, or without cancer history. **(C)** Average numbers of MPO$^+$cit-H3$^+$ cells are shown for each case in each group (n = 10 cases per group). For each case, the average number of MPO$^+$cit-H3$^+$ cells was calculated by counting double-positive cells in five random ×200 microscopic fields. **, P < 0.01; ***, P < 0.001 (Mann-Whitney U test). **(D)** Representative examples of staining. Bar, 100 µm. Error bars in A and C represent SD.

Omental metastasis is decreased in NET-defective, neutrophil-specific *Padi4*$^{-/-}$ mice

To investigate the functional significance of NETs in omental metastasis, we injected groups of adult female neutrophil-specific *Padi4*$^{-/-}$ mice and *Padi4*$^{+/+}$ littermates with ID8 cells i.b. and then evaluated NET formation and the progression of orthotopic tumors in both groups of mice. Flow cytometric analysis of omental tissues revealed no significant difference in the total abundance of neutrophils in the omentum between neutrophil-specific *Padi4*$^{-/-}$ and *Padi4*$^{+/+}$ mice (Fig. S4 E). However, the proportion of omental neutrophils that extruded DNA was substantially reduced in neutrophil-specific *Padi4*$^{-/-}$ mice as compared with *Padi4*$^{+/+}$ littermates (P < 0.001; Fig. 7 A). At 3 wk following i.b. engraftment of ID8 cells, both groups of mice formed primary tumors but no palpable metastasis (Fig. 7, B and C). No significant differences in the size of primary tumors were observed between neutrophil-specific *Padi4*$^{-/-}$ mice and *Padi4*$^{+/+}$ littermates at 3 wk (Fig. 7, B and C) and at 6 wk (Fig. 7, D–G). However, at 6 wk, extensive omental metastasis was detected in *Padi4*$^{+/+}$ mice (Fig. 7, D–G). By contrast, neutrophil-specific *Padi4*$^{-/-}$ mice developed

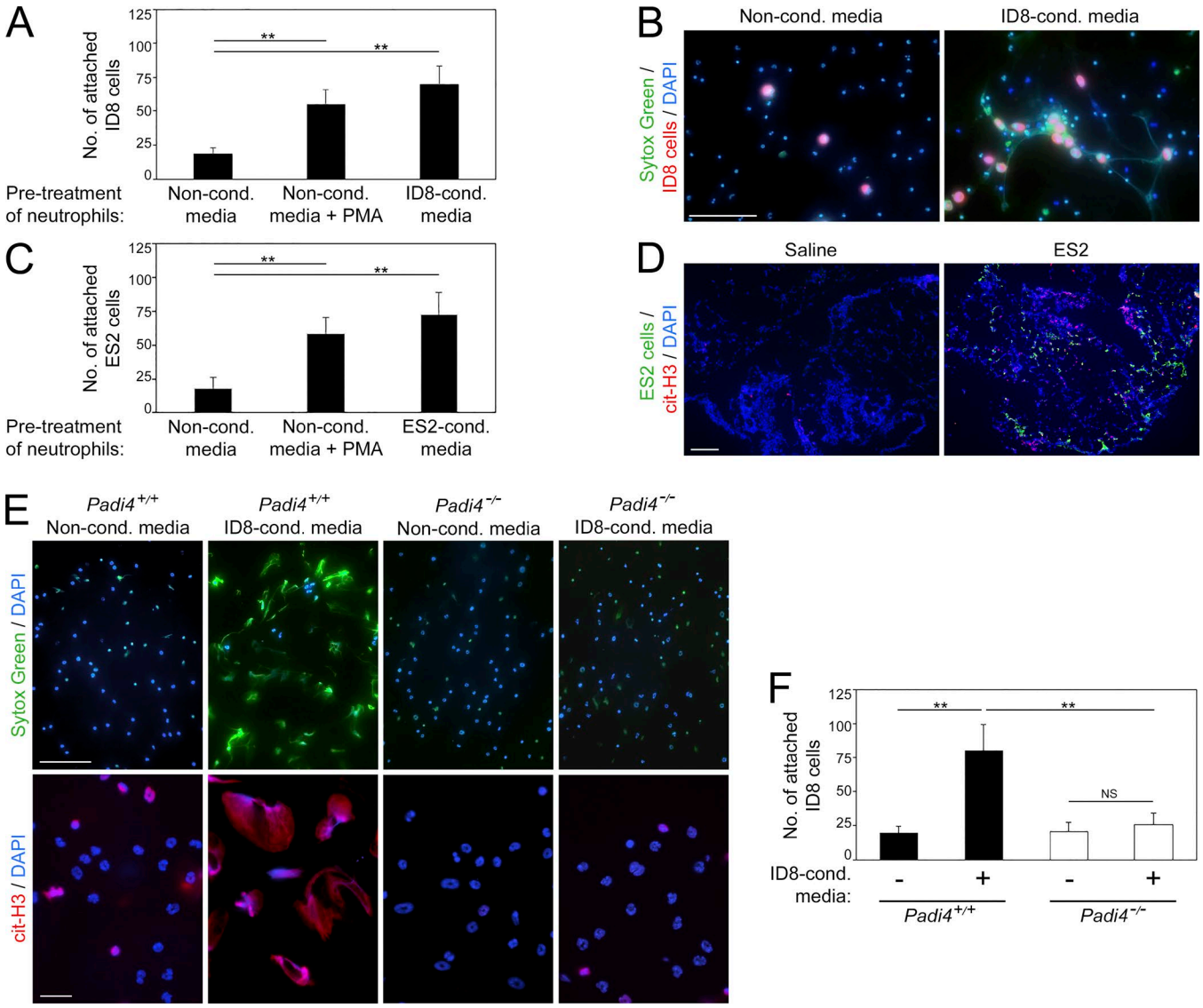

Figure 6. **Ovarian cancer cells attach to NETs. (A and B)** Bone marrow neutrophils of immunocompetent C57BL/6 mice were stimulated for 4 h with ID8-conditioned media or with nonconditioned media without or with addition of PMA. Fluorescently labeled ID8 cells were then seeded onto neutrophils. Attached ID8 cells were counted at 1 h thereafter. **(A)** Shown are means ± SD of three independent experiments, where attached cancer cells were counted in four random ×200 microscopic fields in each experiment. Each experiment used neutrophils from a different donor. **, P < 0.01 (unpaired *t* test). **(B)** Representative image of ID8 cells (red) bound to DNA extruded by neutrophils and stained with Sytox Green dye (green). Bar, 100 µm. **(C)** Human peripheral blood neutrophils were stimulated for 4 h with ES2-conditioned media or with nonconditioned media without or with addition of PMA. ES2 cells were then seeded onto neutrophils and assayed for attachment, as in A. Shown are means ± SD of three independent experiments. Each experiment used neutrophils from a different healthy donor. **, P < 0.01 (unpaired *t* test). **(D)** Omental tissues were collected from nude mice at 6 d following i.p. injection of ES2 cells or saline (n = 3 mice per group). Frozen sections were stained to detect cit-H3 (red) and tumor cells (green). Bar, 100 µm. Shown are representative examples of staining. **(E and F)** Bone marrow neutrophils of neutrophil-specific *Padi4*$^{-/-}$ mice and control siblings were stimulated for 4 h with ID8-conditioned media or with nonconditioned media. **(E)** Neutrophils were stained with Sytox Green dye (green) and with cit-H3 Ab (red). Bars, 100 µm (top) and 20 µm (bottom). **(F)** ID8 cells were seeded onto stimulated neutrophils and assayed for attachment, as in A. Shown are representative images and means ± SD of three independent experiments. **, P < 0.01 (unpaired *t* test).

significantly less omental metastasis (i.e., ∼70% reduction as compared with *Padi4*$^{+/+}$ littermates, P < 0.001; Fig. 7, D–G). These findings indicate that metastasis to the omentum is dependent on the formation of NETs at this site.

Inhibition of NET formation by treatment with PAD4 inhibitor decreases omental colonization

We subsequently tested various pharmacologic agents for the ability to inhibit NET formation. Mouse neutrophils were stimulated with ovarian cancer cell–conditioned media in the absence or presence of CI-amidine, a pan-PAD inhibitor (Knuckley et al., 2010), or GSK484, a recently developed small molecule inhibitor that is highly specific for PAD4 (Lewis et al., 2015). Both of these agents inhibited histone citrullination in neutrophils and also inhibited DNA extrusion (Fig. 8 A). Attachment of ovarian cancer cells to neutrophils was inhibited when neutrophils were pretreated with CI-amidine or GSK484 (P < 0.01; Fig. 8 B). We further evaluated the effect of GSK484 on implantation of

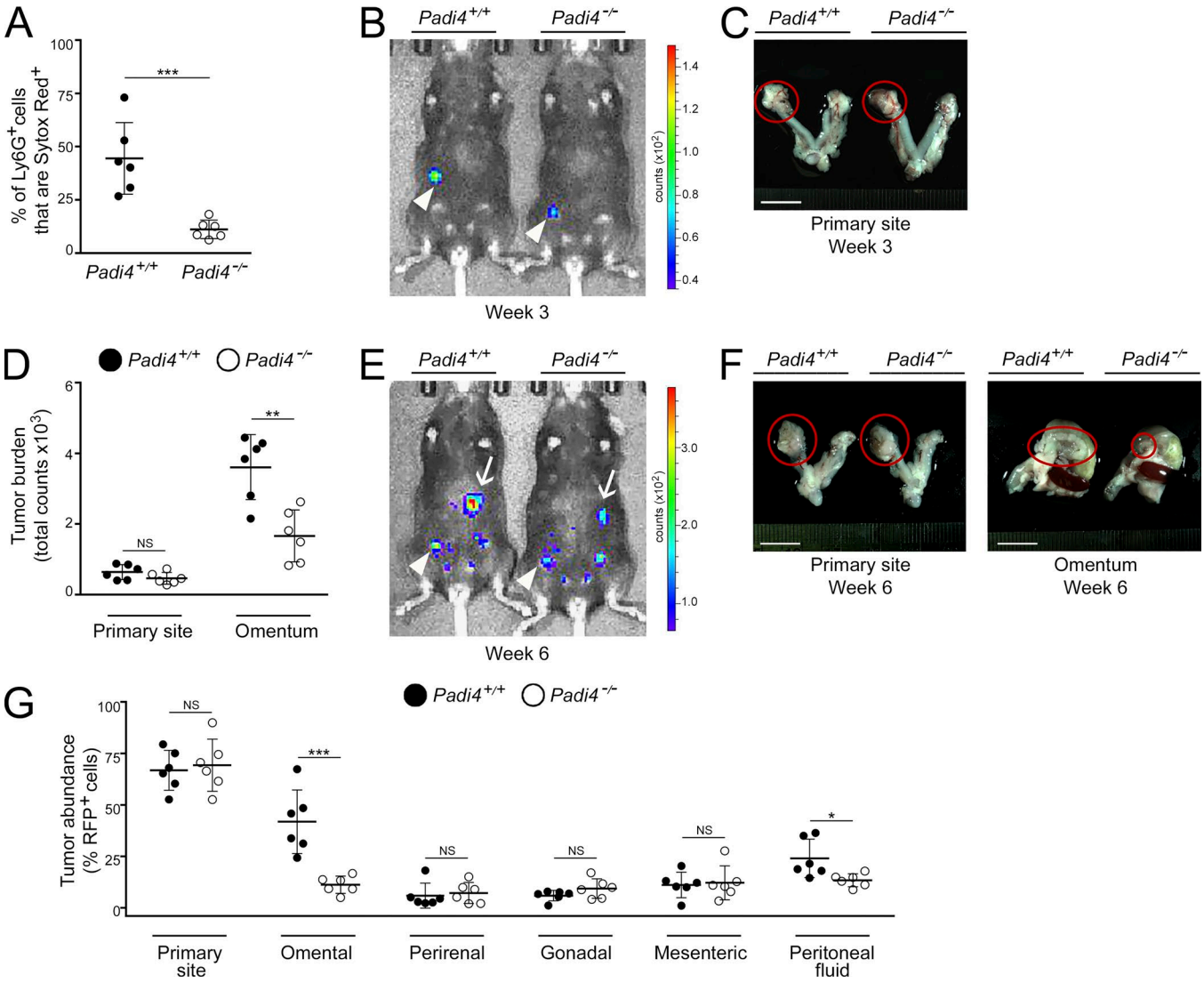

Figure 7. **Omental metastasis is decreased in NET-defective, neutrophil-specific, *Padi4*-deficient mice.** Female neutrophil-specific *Padi4*$^{-/-}$ mice and control siblings were injected i.b. with ID8 cells that express RFP and luciferase and thereafter were evaluated for NET formation and tumor progression. **(A)** At 3 wk, mice in both groups were euthanized (n = 6 mice per group). Fresh omental tissues were stained with Ly6G Ab and Sytox Red dye, and staining was analyzed by flow cytometry. Shown is the proportion of omental Ly6G$^+$ cells that were Sytox Red$^+$ in each mouse of each group. ***, P < 0.001 (unpaired t test). **(B and C)** Representative examples of primary tumors detected at 3 wk by bioluminescence imaging (arrowheads; B) and by light microscopy (circled; C). Bar, 10 mm. **(D–G)** Analysis of tumor progression at 6 wk (n = 6 mice per group). **(D)** Sizes of primary tumors and omental implants detected in each mouse by bioluminescence imaging. **, P < 0.01 (unpaired t test). **(E)** Representative images of mice with primary tumors (arrowheads) and omental implants (arrows). **(F)** Representative images of tumors viewed under light microscopy (circled). Bars, 10 mm. **(G)** Abundance of RFP$^+$ tumor cells in tissues of the primary site, visceral fat tissues, and peritoneal fluid in each mouse, quantified by flow cytometric analysis. *, P < 0.05; ***, P < 0.001 (unpaired t test). Error bars in A, D, and G represent SD.

circulating ovarian cancer cells in vivo. The ES2 i.p. xenograft model was used because ES2 cells do not express PAD4 (Fig. S5 A). GSK484 did not directly affect the viability of ES2 cells in suspension cultures, even at high doses (Fig. S5 B). Female nude mice were injected i.p. with ES2 cells, and at 1 d thereafter were randomized into groups and administered with either saline or GSK484 daily. A nontumor control group of mice was administered saline i.p. daily. Treatment of tumor-bearing mice with GSK484 did not affect the influx of neutrophils into the omentum (Fig. S5 C) but significantly inhibited DNA extrusion by omental neutrophils (P < 0.01; Fig. 8, C and D). Treatment with GSK484 substantially decreased implantation of ovarian cancer cells on the omentum (P < 0.001; Fig. 8, E and F). Colonization of other peritoneal tissues was not increased in GSK484-treated mice, and the abundance of cancer cells in the peritoneal fluid of these mice was decreased as compared with saline-treated mice (P < 0.01; Fig. 8 F). Ascites frequently develops in women with advanced-stage ovarian cancer (Lengyel, 2010) and developed in saline-treated mice with advanced-stage tumors (Fig. S5 D). Ascites was significantly reduced in GSK484-treated mice (P < 0.0001), and a similar reduction was observed when mice were depleted of neutrophils (Fig. S5 D).

To confirm that the decrease in omental colonization observed in GSK484-treated mice is due to inhibition of NETs and

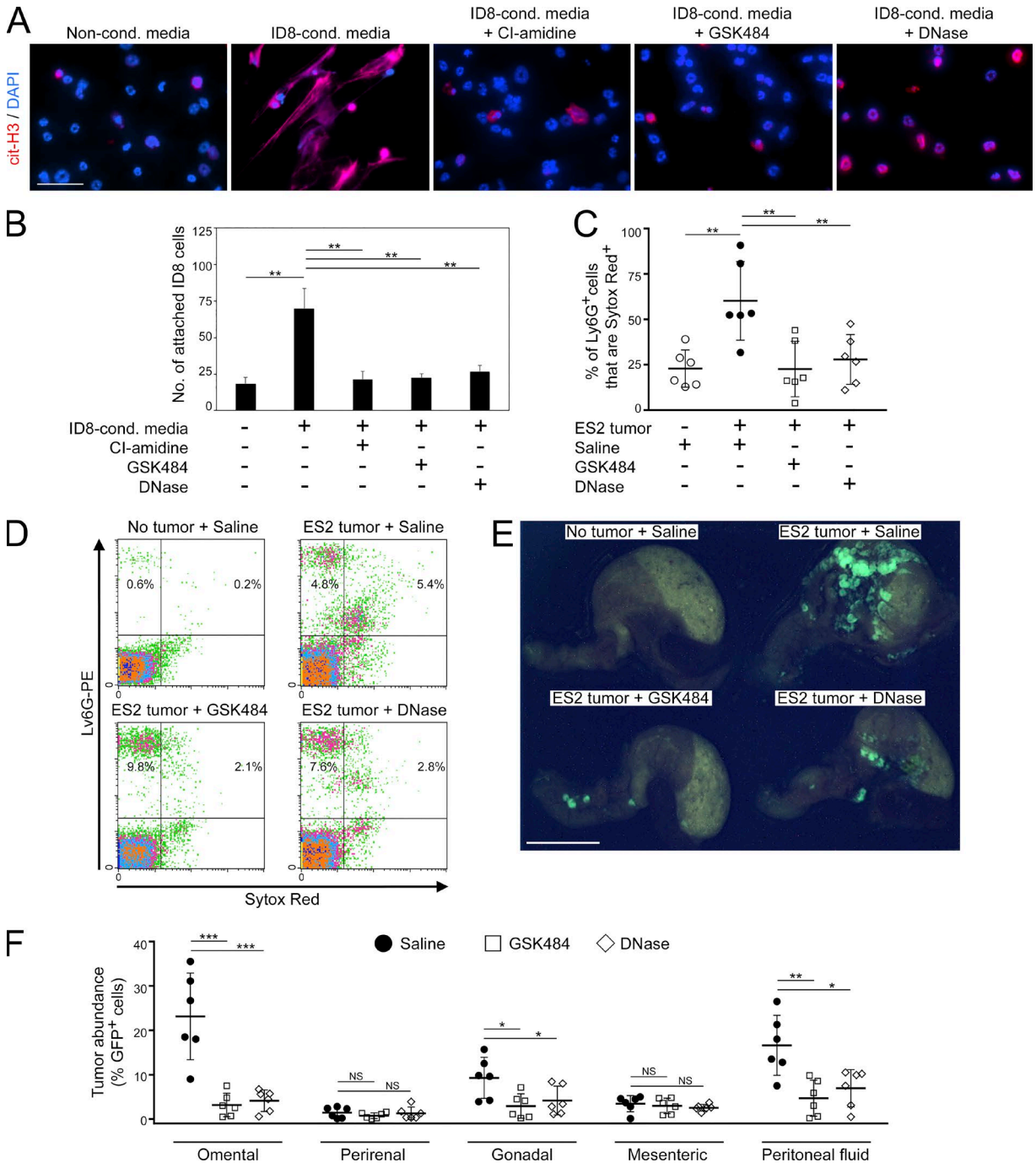

Figure 8. **NET-inhibiting agents decrease omental metastasis. (A)** Normal bone marrow neutrophils of C57BL/6 mice were stimulated for 4 h with non-conditioned media or with ID8-conditioned media without or with addition of CI-amidine (100 µM), GSK484 (10 µM), or DNase (1 µg/ml) and then stained with cit-H3 Ab (red). Bar, 50 µm. Three independent experiments were performed. Shown are representative examples of staining. **(B)** ID8 cells were assayed for attachment to neutrophils that had been prestimulated, as described in A. Shown are means ± SD of three independent experiments, where attached cancer cells were counted in four random ×200 microscopic fields in each experiment. Each experiment used neutrophils from a different donor. **, $P < 0.01$ (unpaired *t* test). **(C–F)** Female nude mice were injected i.p. with GFP-expressing ES2 cells. At 1 d thereafter, mice were randomized into groups and then administered saline, GSK484 (20 mg/kg), or DNase (5 mg/kg) i.p. daily for 9 d. A nontumor control group of mice was administered saline i.p. daily for 9 d. Thereafter, mice in all groups were euthanized ($n = 6$ mice per group). **(C)** Omental tissues were stained with Ly6G Ab and Sytox Red dye, and staining was analyzed by flow cytometry. Shown are the proportion of omental Ly6G$^+$ cells that were Sytox Red$^+$ in each mouse of each group. **, $P < 0.01$ (unpaired *t* test). **(D)** Representative examples of Ly6G and Sytox Red staining analysis. **(E)** Representative images of GFP$^+$ tumors on the omentum. Bar, 10 mm. **(F)** The abundance of GFP$^+$ tumor cells in fat tissues and in peritoneal fluid of each mouse in the ES2 groups was quantified by flow cytometric analysis. *, $P < 0.05$; **, $P < 0.01$; ***, $P < 0.001$ (unpaired *t* test). Error bars in C and F represent SD.

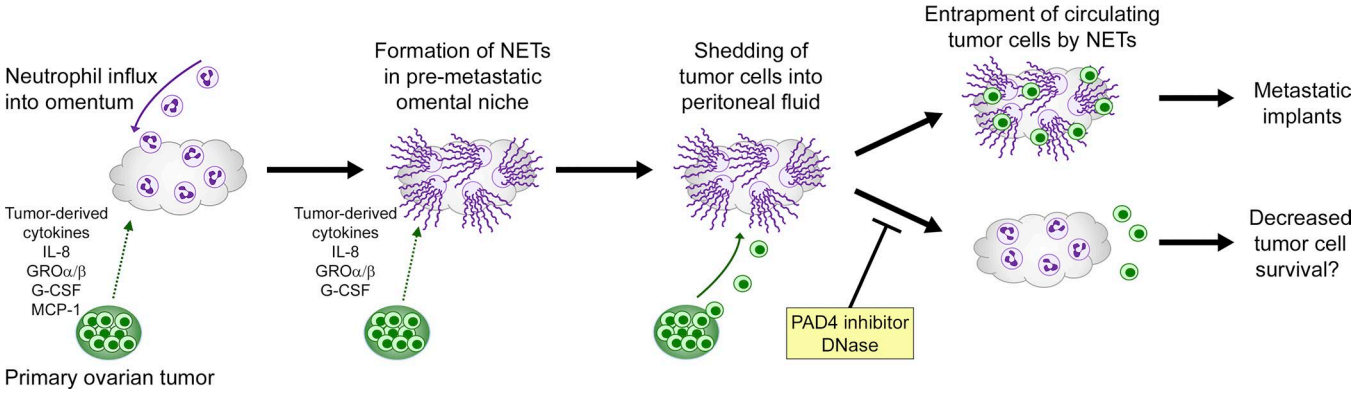

Figure 9. **Proposed mechanism for the metastatic tropism of ovarian cancer for the omentum.** Early-stage ovarian tumors secrete factors that stimulate influx of neutrophils into the premetastatic omental niche and induce these neutrophils to form NETs. Cancer cells that are shed by tumors into the circulating peritoneal fluid become trapped by NETs and then form implants on the omentum.

not to nonspecific effects of this agent, we repeated experiments using recombinant DNase which has been shown to degrade NETs (Brinkmann et al., 2004). Treatment of neutrophils with DNase did not reduce histone citrullination but eliminated extruded DNA (Fig. 8 A). As was observed with GSK484, DNase treatment inhibited attachment of ovarian cancer cells to neutrophils (Fig. 8 B) and did not directly affect cancer cell viability or neutrophil influx into the omentum (Fig. S5, B and C). Treatment of ovarian tumor–bearing mice with DNase eliminated DNA extrusion by omental neutrophils (Fig. 8, C and D) and substantially decreased implantation of cancer cells on the omentum ($P < 0.001$; Fig. 8, E and F). Collectively, these findings demonstrate that inhibition of NETs decreases colonization of the omentum.

Discussion

The i.p. dissemination of ovarian cancer has strong predilection for the omentum and has often been described as a passive process that is governed by the mechanical flow of peritoneal fluid (Tan et al., 2006; Lengyel, 2010; Sodek et al., 2012). However, recent studies of other tumor types that preferentially metastasize to the bone, lung, liver, or brain have shown that metastatic tropism is an orchestrated process in which tumors act cooperatively with various host cells to induce permissive microenvironments at destination sites before colonization (reviewed in Peinado et al., 2017). Virtually nothing is known about the cellular dynamics that establish the premetastatic niche in ovarian cancer and specifically in the omentum. Here, we first identified that early-stage ovarian tumors trigger recruitment of neutrophils to the omentum, predominantly via HEVs in milky spots, and that metastasis to the omentum depends at least in part on this neutrophil influx. The role of neutrophils in ovarian cancer has been unclear. Elevated neutrophil-to-lymphocyte ratio in patients with ovarian cancer has been found to be associated with poor prognosis (Zhou et al., 2017), but the significance of neutrophils in this disease has been questioned by a study that found that ovarian tumor xenografts are not inhibited by treatment with Ab to Gr1 (Robinson-Smith et al., 2007). This interpretation is complicated by the ability of Gr1 Ab to deplete not only neutrophils but also monocytes and subpopulations of lymphocytes and dendritic cells through its recognition of Ly6C in addition to Ly6G (Daley et al., 2008). By administering Ab to Ly6G alone as a more specific approach to deplete neutrophils in mice after primary ovarian tumors have established but before palpable metastasis occurs, we found that omental metastasis was inhibited by ∼70%, whereas primary tumor growth was negligibly affected. We cannot exclude the possibility that at least some of this metastatic inhibition might be due to depletion of PMN-MDSCs that express Ly6G. However, $Ly6G^+$ cells in tumor-bearing mice at the premetastatic stage exhibited the characteristic morphology of neutrophils, and only 1% of these cells were found to express CD115 and CD244 that are reportedly expressed by PMN-MDSCs (Youn et al., 2012). Collectively, these findings strongly implicate the induction by early-stage ovarian tumors of neutrophil influx into the omentum in priming this niche for colonization (Fig. 9).

Neutrophils can exert effects that are either tumor promoting or tumor suppressive, and these effects vary depending on the context (reviewed in Powell and Huttenlocher, 2016). Tumor-promoting properties of neutrophils, such as curtailing adaptive antitumor immunity, appear to predominate at advanced stages of disease, whereas neutrophils in early-stage tumors and in the premetastatic lung niche have been found to be cytotoxic toward cancer cells (Granot et al., 2011; Mishalian et al., 2013). However, neutrophils in the premetastatic lung niche have also been found to promote initiation of breast cancer metastasis by producing leukotrienes that expand a subpopulation of cancer cells with high tumorigenic potential (Wculek and Malanchi, 2015). The ability of neutrophils to form NETs in response to pathological insult was first discovered in microbial infections (Brinkmann et al., 2004) and was subsequently identified in several inflammatory disorders such as lupus (Hakkim et al., 2010). NETs have been detected in patients with advanced-stage metastatic breast cancer (Park et al., 2016), but the dynamics of NET induction in cancer are unclear. In our study, hallmarks of NETs were detected in the omentum of women with early-stage ovarian cancer and of ovarian tumor–bearing mice before palpable colonization of this site but were largely absent in healthy women and tumor-free mice. These findings implicate NET formation in the premetastatic omental niche as an early response by neutrophils to the presence of ovarian tumor in the abdominal cavity (Fig. 9).

Whereas it is well established that tumors secrete factors that stimulate neutrophil mobilization (Powell and Huttenlocher, 2016), the cues that induce neutrophils to form NETs are poorly understood. Classical NETosis depends on generation of reactive oxygen species, and PMA, which is often used to experimentally induce NET formation, potently activates NAPDH oxidase that produces reactive oxygen species (Fuchs et al., 2007). Our findings that depletion of ovarian cancer cell–derived IL-8, G-CSF, GROα, or GROβ decreases NET formation, in addition to reducing neutrophil chemotaxis, are consistent with the ability of these cytokines to potentiate respiratory burst (Nathan, 1989; Geiser et al., 1993) and indicate that at least some cytokines may stimulate both neutrophil mobilization and NETosis. On the other hand, our finding that depletion of MCP-1 did not significantly decrease NETosis is consistent with the reported inability of MCP-1 to stimulate respiratory burst in neutrophils (Rollins et al., 1991). The ability of a single cytokine to optimally trigger respiratory burst has been controversial (Nathan, 1989; Mitchell et al., 2003). Our findings that depletion of IL-8, G-CSF, GROα, or GROβ did not completely abrogate NET formation suggest that these cytokines cooperate with one another and other factors to optimally induce this process. One candidate could be tumor necrosis factor–α (TNF-α) which, although not detected in the model used in our study, potentiates respiratory burst (Nathan, 1989). TNF-α is more highly expressed in high-grade ovarian carcinomas than in low-malignant-potential tumors (Naylor et al., 1993). Circulating levels of IL-8 are also higher in women with ovarian carcinoma than in those with low-malignant-potential tumor (Aune et al., 2012). Notably, we detected a higher number of NET-positive neutrophils in the omentum of women with early-stage HGSC than in those with early-stage SLMP. These findings support the notion that NET formation at the destination site is reflective of the metastatic potential of a tumor and is stimulated by tumor-derived inflammatory factors. It is possible that stroma-derived factors could also promote neutrophil recruitment and/or NETosis. For example, IL-8 and MCP-1 are expressed by omental adipocytes (Nieman et al., 2011). However, it is unlikely that T cell–derived factors play a significant role in stimulating neutrophil recruitment or NET formation because these processes were induced in the omentum of nude mice with early-stage tumors.

NET formation was originally identified as a mechanism by which neutrophils capture and disarm microbes (Brinkmann et al., 2004). NETs have been implicated in promoting tumor progression by reports that NETs bind lung cancer cells (Cools-Lartigue et al., 2013) and that breast cancer metastasis in mice is inhibited by DNase (Park et al., 2016). However, the significance of NETs in directing metastatic tropism and the extent to which NETs account for the tumor-promoting ability of neutrophils are unclear. We found that ovarian cancer cells bind to NET-positive neutrophils and that omental metastasis but not primary tumor growth was profoundly reduced (i.e., by ∼70%) in neutrophil-specific *Padi4*$^{-/-}$ mice that are defective in NET formation but have normal leukocyte counts and neutrophil chemotactic responses. Treatment of NET-competent mice with NET-inhibiting agents also reduced omental colonization to a similar extent without altering neutrophil influx. Our findings that omental metastasis was inhibited by ∼70% in neutrophil-depleted mice suggest that NET formation substantially accounts for the tumor-promoting ability of neutrophils. We cannot exclude the possibility that neutrophils might also promote omental metastasis by NET-independent mechanisms or that some cancer cell loss occurs through NET-mediated cytotoxicity. However, our findings support a model in which metastatic tropism of ovarian cancer is orchestrated first by the induction of NET formation in the premetastatic omental niche and second by NET-mediated entrapment of circulating cancer cells at this site (Fig. 9). Intriguingly, NET-defective neutrophil-specific *Padi4*$^{-/-}$ mice and also NET-competent mice treated with NET-inhibiting agents showed decreased abundance of cancer cells in the peritoneal fluid and no increased extraomental involvement. It might be expected that inhibiting implantation of cancer cells at one site would increase numbers of circulating cancer cells and colonization of other sites. Our findings could be explained in part by the dynamics of i.p. seeding of ovarian cancer. This process of dissemination is a self-perpetuating cycle in which implants form, grow, and shed cancer cells that then form new implants (Sodek et al., 2012). A higher number of tumor implants could give rise to a higher number of circulating cancer cells. NETs might also promote tumor progression by other mechanisms. NETs contain proteinases that remodel the local microenvironment and can lead to tissue damage (Brinkmann et al., 2004; Albrengues et al., 2018). Extracellular histones can also induce endothelial cell death (Xu et al., 2009). Other host cells that are recruited to NET-rich sites of damage might secrete factors that stimulate growth of tumor implants and prevent anoikis in circulating cancer cells. NET-inhibiting agents might decrease peritoneal carcinomatosis by not only blocking entrapment of cancer cells in the omental niche but also quenching NET-mediated effects on other stromal cells that foster a tumor-permissive microenvironment.

Although our study demonstrates that NET-inhibiting agents reduce omental metastasis, it could be argued that these agents have limited utility for ovarian cancer therapy, because omentectomy is a standard procedure for staging and treatment of this disease irrespective of omental involvement. However, several studies have questioned the therapeutic benefit of omentectomy in the absence of overt metastasis and have highlighted the need to preserve the protective function of the uninvolved omentum. Two independent studies of women with stage I/II ovarian cancer found that omentectomy had no significant or only modest association with improved survival (Cress et al., 2011; McNally et al., 2015). A study that used rat models of ovarian cancer found that survival was not substantially improved when the omentum was removed before seeding of this site (Yokoyama et al., 2012). NET-inhibiting agents might be most beneficial in a setting where early-stage ovarian cancer is treated without omentectomy. These agents might also improve outcomes in patients with ovarian cancer by alleviating common comorbidities such as pulmonary embolism and sepsis. NETs stimulate thrombus formation and can cause organ damage, and these effects can be alleviated by treatment with DNase (Fuchs et al., 2010; McDonald et al., 2012). Neutropenia is a common side effect of chemotherapy and occurs in ∼60% of ovarian cancer patients who receive platinum-taxane chemotherapy (Hashiguchi et al., 2015). Our finding that G-CSF, which is used for prophylaxis of neutrope-

nia, potentiates NET formation raises a cautionary note that the prophylactic benefit of G-CSF should be weighed against its stimulatory effect on metastasis. Indeed, administration of G-CSF for prophylaxis has been found to not significantly improve ovarian cancer patient survival (Matsui et al., 2014).

In summary, our findings support a model in which the influx of neutrophils and formation of NETs in the premetastatic omental niche promotes a microenvironment that is conducive for preferential implantation of ovarian cancer cells at this site. Our study also demonstrates that inhibiting NET formation decreases omental metastasis. Further studies of this intriguing host defense mechanism could yield new insights into improving ovarian cancer treatment and ameliorating common comorbidities.

Materials and methods

Reagents

Sources of Ab for the indicated applications were as follows: for flow cytometry, Ly6G-PE, F4/80-PE, Gr1-PE, CD11b-peridinin-chlorophyll-protein (PerCP), CD115-PerCP, CD244.2-PerCP, CD11b-allophycocyanin, and isotype controls (BioLegend); for immunohistochemistry, CD31, Ly6G, neutrophil elastase, human nucleoli, cit-H3 (Abcam), PNAd (Santa Cruz Biotechnology), MPO (R&D Systems), isotype controls (Thermo Fisher Scientific), and Alexa Fluor 488– and Alexa Fluor 594–conjugated secondary Ab (Life Technologies); and for neutralization, Ly6G (clone 1A8), isotype controls (BioXcell), and human IL-8, MCP-1, GROα, pan-GRO, and G-CSF (R&D Systems). Sources of chemicals were as follows: Sytox Green and Sytox Red (Life Technologies); PMA and DAPI (Sigma-Aldrich); CI-amidine and GSK484 (Cayman Chemical); recombinant DNase I and collagenase type II (Worthington Biochemical Corp.); and D-luciferin (Gold Biotechnology).

Plasmids

To generate the pMSCV-Luc-tGFP retroviral construct that coexpresses luciferase and turboGFP (tGFP), the EGFP sequence was removed from the MSCV-IRES-GFP vector (gift from Tannishtha Reya [University of California, San Diego, San Diego, CA]; Addgene plasmid 20672) by digestion with *Nco* I and *Sal* I and replaced with the tGFP sequence that was amplified from pGFP-V-RS vector (Origene). The luciferase sequence was isolated from pGL3 basic vector (Promega) by digestion with *Bgl* II and *Sal* I and subcloned into the MSCV-IRES-GFP vector 5′ of the IRES sequence. To generate the pMSCV-Luc-RFP retroviral construct that coexpresses luciferase and RFP, the luciferase sequence was subcloned into the pMSCV-pBabeMCS-IRES-RFP vector (gift from Martine Roussel and Charles Sherr [St. Jude Children's Research Hospital, Memphis, TN]; Addgene plasmid 33337). The pQCXIP-VEGFA121 construct that expresses the 121–amino acid isoform of vascular endothelial growth factor (VEGF) was a gift from Michael Grusch (Medical University of Vienna, Vienna, Austria; Addgene plasmid 73017).

Cancer cell culture, transfection, and conditioned media

Cancer cell lines were authenticated by short tandem repeat analysis by the MD Anderson Cancer Center Characterized Cell Line Core Facility and verified to be free of mycoplasma contamination. Parental ES2 cells were purchased from American Type Culture Collection and were cultured in McCoy's 5A medium (Corning) containing 10% FBS and penicillin-streptomycin. ES2 cells that stably express tGFP have been previously described (Ko et al., 2012). ID8 cells have been previously described (Roby et al., 2000) and were provided by Katherine Roby (University of Kansas Medical Center, Kansas City, KS). ID8 cells were cultured in DMEM (Corning) containing 10% FBS and penicillin-streptomycin. To generate ID8 lines that stably coexpress either luciferase and tGFP or luciferase and RFP, Ampho-293 cells (purchased from American Type Culture Collection) were transfected with pMSCV-Luc-tGFP or pMSCV-Luc-RFP plasmids by using Lipofectamine 2000 (Thermo Fisher Scientific). Supernatants were harvested at 2 d thereafter and used to infect ID8 cells. At 3 d after infection, tGFP- or RFP-expressing ID8 cells were sorted using a MoFlo Astrios Cell Sorter (Beckman Coulter). Because generation of xenografts from ID8 cells is enhanced when ID8 cells stably express VEGF (Zhang et al., 2002), ID8 cells were also infected with pQCXIP-VEGFA121 retrovirus and then selected with puromycin (0.5 µg/ml). To generate cancer cell–conditioned media, ES2 and ID8 cells were cultured at subconfluence in RPMI 1640 medium (Corning) containing 0.2% BSA for 2 d. Media were then collected and filtered through a 0.45-µm filter. Where indicated, conditioned media were depleted of cytokines by immunoprecipitation (IP) using neutralizing Ab at concentrations described in Fig. S3 C. Nonconditioned RPMI 1640 medium containing 0.2% BSA was used as a negative control in in vitro assays.

Human tissues

All studies using human tissues were reviewed and approved by the Institutional Research Boards of the University of Texas MD Anderson Cancer Center and the University of Chicago and received patients' informed consent. This study only used residual tissues that were delinked from identifiers. FFPE sections of omental tissues of women with a confirmed diagnosis of FIGO stage III HGSC, FIGO stage I/II HGSC, or FIGO stage I/II SLMP and of women with no cancer history who had undergone abdominal cerclage were obtained from the Ovarian Cancer Tumor Bank at the University of Chicago. Women with infections were excluded from all three groups. Normal peritoneal fibroblasts were isolated as previously described (Kenny et al., 2007). Normal fallopian tube tissue was obtained from the MD Anderson Cancer Center Gynecological Tumor Bank. Residual blood samples from healthy adult volunteers were provided by the MD Anderson Cancer Center Blood Bank.

Mouse strains

Female nude and NSG mice were purchased from the MD Anderson Cancer Center Animal Facility. Wild-type C57BL/6 mice were purchased from The Jackson Laboratory (stock no. 000664). *Padi4*$^{fl/fl}$ mice (*Padi4*-floxed) have been previously described (Hemmers et al., 2011) and were purchased from The Jackson Laboratory (stock no. 026708, B6(Cg)-*Padi4*$^{tm1.2Kmow}$/J). MRP8-Cre-ires/GFP transgenic mice (henceforth described as MRP8-Cre) have been previously described (Passegué et al., 2004) and were purchased from The Jackson Laboratory (stock no. 021614, B6.Cg-Tg(S100A8-cre,-EGFP)1Ilw/J). Heterozygous MRP8-Cre

mice were crossed with homozygous *Padi4*$^{fl/fl}$ mice to generate heterozygous MRP8-Cre/*Padi4*$^{fl/+}$ progeny that were then crossed with *Padi4*$^{fl/fl}$ mice. Of the resultant progeny, female MRP8-Cre/*Padi4*$^{fl/fl}$ mice were used as the test group (referred to as neutrophil-specific *Padi4*$^{-/-}$). Female littermates that lacked MRP8-cre were used as controls. Genotypes were validated by genomic PCR using primers specified by The Jackson Laboratory. All animals that were bred and/or used in this study were housed under specific pathogen–free conditions.

Animal studies

All animal studies were reviewed and approved by the Institutional Animal Care and Use Committee of the University of Texas MD Anderson Cancer Center. All procedures on animals were performed under aseptic conditions and using sterile instruments. To generate orthotopic tumors, 8–9-wk-old female C57BL/6 mice were anesthetized by inhalation of 2–4% isofluorane in oxygen. A small incision was made on the back of each mouse above the left ovarian fat pad to expose the oviduct and ovary. ID8 cells (10^6 cells suspended in 10 µl sterile PBS) were injected into the i.b. space with a 26-gauge needle and Hamilton syringe. The incision was then closed using sterile sutures and wound clips. Control siblings were injected i.b. with 10 µl PBS by the same procedure. To prevent infections, mice were administered Baytril (0.17 mg/ml in drinking water) for 1 wk before and 3 wk following injection. To generate i.p. xenografts, ID8 cells were injected i.p. into 6–7-wk-old female C57BL/6 and NSG mice, and ES2 cells were injected i.p. into 4-wk-old female nude mice (10^6 cells suspended in 100 µl PBS). Control female siblings were injected i.p. with 100 µl PBS. To deplete neutrophils, C57BL/6 mice were injected i.b. with ID8 cells and at 3 wk thereafter were randomized into groups that were then administered either Ly6G Ab or control Ig (200 µg per mouse) i.p. twice a week for 3 wk. The same doses of Ab were administered i.p. to nude mice at 3 d and 1 d before injection of ES2 cells. To test effects of NET-inhibiting agents, nude mice were injected i.p. with ES2 cells and at 1 d thereafter randomized into groups that were then administered either PBS, GSK484 (20 mg/kg body weight), or DNase (5 mg/kg body weight) i.p. daily for 9 d. These doses have been found to be nontoxic in mice (Meng et al., 2012; Moore et al. 2015. The American College of Rheumatology/Association of Rheumatology Health Professionals Annual Meeting. Abstr. 1769). A nontumor group of nude mice was administered PBS i.p. daily for 9 d. Where indicated, nude mice were injected i.p. with ES2 cells and administered PBS, GSK484 (20 mg/kg body weight, daily), or Ly6G Ab (200 µg per mouse, twice a week) for 18 d. Bioluminescence imaging was performed to detect primary tumors and metastases at the time points indicated in the text. Mice were anesthetized; injected i.p. with D-luciferin (150 mg/kg body weight); and at 5 to 30 min thereafter, imaged by using an IVIS Lumina 200 imaging system (Caliper LifeSciences). Imaging data were acquired and analyzed by using Living Image software (Caliper LifeSciences). Tumor sizes were calculated from total counts in regions defined by emitted signals. Mice were euthanized by CO_2 asphyxiation at time points indicated in the text, and tissues were harvested. GFP-expressing tumors were visualized under an MZML III stereomicroscope with a fluorescein filter set (Leica Microsystems). Ascites was collected from the abdominal cavity, and volumes were measured using a micropipette. Peripheral blood samples (200 µl) were drawn retro-orbitally from anesthetized mice and collected in EDTA-coated tubes. In terminal experiments, blood samples were collected from mice by cardiac puncture immediately following euthanasia. CBC tests were performed using an ADVIA 120 Hematology System (Siemens).

Flow cytometry

To quantify GFP$^+$ or RFP$^+$ tumor cells in mouse tissues, each tissue was minced with scissors, suspended in Hanks' Balanced Salt Solution containing calcium and magnesium, and incubated with collagenase type II (1 mg/ml) at 37°C for 30 min with shaking. Tissues were then passed through 70-µm nylon mesh (BD Biosciences), to further disaggregate tissues and exclude fat cells. Cells in peritoneal fluid were collected from mice by gently flushing the abdominal cavity with PBS. Cells from fluid and tissues were pelleted, washed with PBS, and acquired. Percentages of GFP$^+$ or RFP$^+$ cells were calculated within the gated population of live cells defined by forward- and side-scatter analysis. A minimum of 10,000 gated events was analyzed for each sample. To quantify myeloid cells in tissues, each tissue was minced with scissors, suspended in PBS containing 1% BSA, and passed through 70-µm nylon mesh. Cells were pelleted, incubated with Ly6G-PE or F4/80-PE Ab (2 µg/ml) and CD11b-PerCP Ab (2 µg/ml) at 4°C for 30 min, then washed, fixed with 4% paraformaldehyde, and acquired. To analyze DNA extrusion in neutrophils, tissues were disaggregated and incubated with Ly6G-PE Ab as described above. Cells were then stained with Sytox Red dye (5 nM) for 5 min, washed, fixed, and acquired. To evaluate neutrophil depletion in mice following administration of Ly6G Ab, peripheral blood mononuclear cells were stained with Gr1-PE Ab in combination with CD11b-PerCP Ab to avoid false-negative results, because the Ly6G depleting Ab may mask the Ly6G epitope. Where indicated, cells were also stained with Ly6G-PE, CD11b-allophycocyanin, and either CD115-PerCP or CD244-PerCP (2 µg/ml). Acquisition and analysis of flow cytometry data were performed using a FACSCalibur flow cytometer equipped with CellQuest Pro software (BD Biosciences) and an Accuri C6 Plus flow cytometer equipped with Accuri C6 Plus software (BD Biosciences).

Neutrophil isolation and in vitro NET induction

Neutrophils were isolated from adult human peripheral blood by density gradient separation using dextran-Ficoll-Paque Premium (GE Healthcare) and from bone marrow of 7–8-wk-old mice using Percoll (GE Healthcare). Isolated neutrophils were confirmed to be of >95% purity by flow cytometric analysis of staining of neutrophil markers. Unless noted otherwise, neutrophils were cultured in RPMI 1640 medium containing 0.2% BSA. To induce NET formation, freshly isolated neutrophils were seeded in 8-well chamber slides (Sigma-Aldrich; 2×10^4 cells per well) and allowed to rest for 1 h. Thereafter, neutrophils were incubated for 4 h in cancer cell–conditioned media or in nonconditioned media. Where indicated, PMA (500 nM), CI-amidine (100 µM), GSK484 (10 µM), or DNase I (1 µg/ml) was added to conditioned media. To detect extruded DNA, neutrophils were stained with Sytox Green dye (5 nM) for 5 min. To detect cit-H3, neutrophils

were fixed with 1% paraformaldehyde, permeabilized in 0.1% Triton X-100 for 5 min and washed. Cells were then incubated with Ab to cit-H3 (10 µg/ml) at 37°C for 1 h, washed, and incubated with Alexa Fluor 594–conjugated secondary Ab. Cells were counterstained with DAPI, mounted, and viewed under a Nikon 80i fluorescence microscope. For each assay, three independent experiments were performed where each experiment used neutrophils from a different donor. Scoring of staining is described in the figure legends.

Immunohistochemistry and cytological staining

For whole-mount staining, mouse omental tissues were fixed in 2% paraformaldehyde at 4°C for 4 h, followed by incubation in blocking buffer (PBS containing 10% goat serum and 0.01% Tween-20) for 1 h. Tissues were then incubated with Ab to PNAd (4 µg/ml) and to CD31 (20 µg/ml) in blocking buffer at 4°C for 48 h. Thereafter, tissues were washed three times with PBS containing 0.05% Tween-20 and incubated with Alexa Fluor 488– and Alexa Fluor 594–conjugated secondary Abs in blocking buffer at 4°C for 4 h. Tissues were then washed, counterstained with DAPI, and viewed under a Zeiss LSM710 confocal microscope. Images were processed by using Zen 2.31 SP (Black edition) software (Zeiss). For staining frozen sections, mouse omental tissues were frozen in Optimal Cutting Temperature Compound (Thermo Fisher Scientific) and cut into 10-µm sections. Slides were blocked and incubated overnight at 4°C with Ab to PNAd (4 µg/ml), CD31 (20 µg/ml), Ly6G (10 µg/ml), or cit-H3 (10 µg/ml). To detect human cancer cells in mouse tissues, slides were incubated with Ab specific to human nucleoli (1 µg/ml). Following incubation with primary Ab, slides were washed with PBS, incubated for 45 min with Alexa Fluor 488– or Alexa Fluor 594–conjugated secondary Abs, and washed again. Slides were then counterstained with DAPI and viewed under a Nikon 80i fluorescence microscope. Images were captured by using NIS-Elements software (Nikon). For staining FFPE human omental tissue sections, slides were deparaffinized in xylene, rehydrated in alcohol, boiled in 10 mM sodium citrate (pH 7.0) to retrieve antigens, and then incubated in blocking buffer. Slides were incubated with Ab to PNAd (4 µg/ml) or to neutrophil elastase (10 µg/ml) overnight at 4°C, and staining was detected by streptavidin-biotin-peroxidase and 3, 3′-diaminobenzidine (Dako). Slides were then counterstained with H&E (Vector Labs). In other experiments, slides were incubated with Ab to MPO (15 µg/ml) and cit-H3 (20 µg/ml), followed by washing and incubation with Alexa Fluor 488– and Alexa Fluor 594–conjugated secondary Abs. Scoring of staining is described in the figure legends. $Ly6G^+$ and $F4/80^+$ cells were isolated from peripheral blood by using anti-Ly6G and anti-F4/80 microbeads (Miltenyl Biotec) according to the manufacturer's instructions, transferred onto slides by cytocentrifugation, and stained with Giemsa dye (Sigma-Aldrich).

Chemotaxis assay

To evaluate neutrophil chemotaxis, nonconditioned medium or cancer cell–conditioned medium was added to the lower well of 96-well CytoSelect 3-µm-pore migration chambers (Cell Biolabs). Human or mouse neutrophils (2.5×10^5 cells) were seeded in the upper well. At 2 h thereafter, migrating cells on the lower surface of the membrane separating the chambers were stained with CyQuant dye (Cell Biolabs) following the manufacturer's instructions. Migrating cells were quantified by measuring fluorescence using a Synergy HT Plate reader (Biotek). Three independent experiments were performed in which mean fluorescence intensity was evaluated in four replicate wells in each experiment and where each experiment used neutrophils from a different donor.

Cell attachment assay

To evaluate attachment of cancer cells to neutrophils, neutrophils were initially seeded in 96-well plates (10^4 cells per well) and incubated for 4 h with cancer cell–conditioned media or with nonconditioned media. Where indicated, PMA (500 nM), CI-amidine (100 µM), GSK484 (10 µM), or DNase I (1 µg/ml) was added to the medium. Thereafter, neutrophils were gently washed, and fresh nonconditioned medium was added to all wells. Cancer cells that expressed GFP or that were labeled with PKH26 red fluorescent cell linker dye (Sigma-Aldrich) according to manufacturer's instructions were then seeded onto neutrophils (2×10^4 cancer cells per well). At 1 h thereafter, wells were gently washed to remove unattached cancer cells. Attached cancer cells were viewed and counted under a fluorescence microscope. Where indicated, cultures were stained with Sytox Green dye and DAPI, as described for immunofluorescence staining studies. Three independent experiments were performed in which attached cancer cells were counted in four random ×200 microscopic fields in each experiment and where each experiment used neutrophils from a different donor.

Cell viability assay

To evaluate the direct effect of NET-inhibiting agents on viability of ovarian cancer cells, ES2 cells were seeded in 96-well plates (8×10^3 cells per well) that were precoated with poly(2-hydroxyethyl methacrylate) (Sigma-Aldrich) as described in previous studies (Ko et al., 2010). At 1 d thereafter, CI-amidine, GSK484, or DNase I was added at concentrations indicated in Fig. S5 B, and cells were incubated for a further 2 d. Thereafter, cell viability was measured by the 3-(4,5-dimethylthiazol-2-yl)-2,5-diphenyl tetrazolium bromide (MTT) assay (Roche) according to manufacturer's instructions. Three independent assays were performed.

Ab array analysis and ELISA

Cytokines were detected in ovarian cancer cell–conditioned media by using the Human Cytokine Antibody Array (Abcam). Membranes were incubated with conditioned media at 4°C for 16 h and then incubated with Ab and visualized according to the manufacturer's instructions. Signals on membranes were verified in two independent experiments. Levels of IL-8, MCP-1, GROα, GROβ, and G-CSF in conditioned media were assayed by ELISA using kits purchased from R&D Systems, according to the manufacturer's instructions. Levels of each cytokine were assayed in three independent sets of conditioned medium and normalized to total cellular protein content.

qRT-PCR

Total RNA was isolated from tissues and cells using TRIzol reagent (Thermo Fisher Scientific). Reverse transcription was performed

using SuperScript II (Invitrogen). PCR reactions were performed in a CFX96 Real-Time PCR Detection System (Bio-Rad), using SYBR Green qPCR core reagent according to the manufacturer's instructions, with the following primers: human *PADI4*, forward, 5′-GCACAACATGGACTTCTACGTGG-3′, and reverse, 5′-CACGCT GTCTTGGAACACCACA-3′; and mouse *Padi4*, forward, 5′-CAG GAGGTGTACGTGTGCA-3′, and reverse, 5′-CTCTGTCCCTCGGGG AGTC-3′. *RPL32* transcript and 18S rRNA levels were used as controls for normalization and were detected in human and mouse tissues/cells using the following primers: *RPL32/Rpl32*, forward, 5′-CCTTGTGAAGCCCAAGATCG-3′, and reverse, 5′-TGCCGGATG AACTTCTTGGT-3′; and *18S*, forward, 5′-CTCAACACGGGAAAC CTCAC-3′, and reverse, 5′-CGCTCCACCAACTAAGAACG-3′. Three independent PCR reactions were performed for each transcript.

Statistics

Statistical analysis was performed using Statistica 13.1 (StatSoft Inc.) and Prism 6 software (GraphPad Software, Inc.). Significance of data in in vitro and in vivo assays was assessed by unpaired or paired (where indicated) two-tailed Student's *t* test. Data represent means ± SD. Based on the variance of xenograft growth observed in preliminary studies, six mice per group was calculated as the minimum number to detect a >50% difference in data values between groups at a significance of $P < 0.05$ and with 90% probability. Significance of data between groups of patients was assessed by Mann–Whitney *U* test. P values of <0.05 were considered significant.

Online supplementary information

Fig. S1 shows kinetics of tumor implant formation in ID8 orthotopic and ES2 i.p. models. Fig. S2 shows the abundance and characteristics of neutrophils and effects of neutrophil depletion in ES2 i.p. models. Fig. S3 demonstrates that ovarian cancer cells secrete factors that induce neutrophils to mobilize and form NETs. Fig. S4 shows characterization of neutrophil-specific *Padi4*$^{-/-}$ mice. Fig. S5 shows the effects of NET-inhibiting agents on ovarian cancer cell viability, neutrophil abundance, and ascites.

Acknowledgments

We thank Hironari Akasaka (University of Texas MD Anderson Cancer Center) for helpful discussions. We thank the animal, flow cytometry, and characterized cell line core facilities supported by the MD Anderson Cancer Center core grant NCI CA16672 for technical assistance.

This work was supported by National Institutes of Health grants CA217931 (to H. Naora), CA207034 (to H. Naora), and CA169604 (to E. Lengyel).

The authors declare no competing financial interests.

Author contributions: W. Lee and H. Naora conceived the study and designed the experiments. W. Lee, S.Y. Ko, M.S. Mohamed, and H. Naora performed the experiments. H.A. Kenny and E. Lengyel provided clinical specimens. W. Lee, S.Y. Ko, and H. Naora analyzed the data. W. Lee and H. Naora wrote the manuscript. S.Y. Ko, H.A. Kenny, and E. Lengyel edited the manuscript. H. Naora supervised the study.

Submitted: 21 June 2018
Revised: 9 October 2018
Accepted: 15 November 2018

References

Abram, C.L., G.L. Roberge, Y. Hu, and C.A. Lowell. 2014. Comparative analysis of the efficiency and specificity of myeloid-Cre deleting strains using ROSA-EYFP reporter mice. *J. Immunol. Methods.* 408:89–100. https://doi.org/10.1016/j.jim.2014.05.009

Albrengues, J., M.A. Shields, D. Ng, C.G. Park, A. Ambrico, M.E. Poindexter, P. Upadhyay, D.L. Uyeminami, A. Pommier, V. Küttner, et al. 2018. Neutrophil extracellular traps produced during inflammation awaken dormant cancer cells in mice. *Science.* 361:eaao4227. https://doi.org/10.1126/science.aao4227

Aune, G., A.K. Stunes, A.M. Lian, J.E. Reseland, S. Tingulstad, S.H. Torp, and U. Syversen. 2012. Circulating interleukin-8 and plasminogen activator inhibitor-1 are increased in women with ovarian carcinoma. *Results Immunol.* 2:190–195. https://doi.org/10.1016/j.rinim.2012.10.003

Brinkmann, V., U. Reichard, C. Goosmann, B. Fauler, Y. Uhlemann, D.S. Weiss, Y. Weinrauch, and A. Zychlinsky. 2004. Neutrophil extracellular traps kill bacteria. *Science.* 303:1532–1535. https://doi.org/10.1126/science.1092385

Buscher, K., H. Wang, X. Zhang, P. Striewski, B. Wirth, G. Saggu, S. Lütke-Enking, T.N. Mayadas, K. Ley, L. Sorokin, and J. Song. 2016. Protection from septic peritonitis by rapid neutrophil recruitment through omental high endothelial venules. *Nat. Commun.* 7:10828. https://doi.org/10.1038/ncomms10828

Clark, R., V. Krishnan, M. Schoof, I. Rodriguez, B. Theriault, M. Chekmareva, and C. Rinker-Schaeffer. 2013. Milky spots promote ovarian cancer metastatic colonization of peritoneal adipose in experimental models. *Am. J. Pathol.* 183:576–591. https://doi.org/10.1016/j.ajpath.2013.04.023

Cohen, C.A., A.A. Shea, C.L. Heffron, E.M. Schmelz, and P.C. Roberts. 2013. The parity-associated microenvironmental niche in the omental fat band is refractory to ovarian cancer metastasis. *Cancer Prev. Res. (Phila.).* 6:1182–1193. https://doi.org/10.1158/1940-6207.CAPR-13-0227

Cools-Lartigue, J., J. Spicer, B. McDonald, S. Gowing, S. Chow, B. Giannias, F. Bourdeau, P. Kubes, and L. Ferri. 2013. Neutrophil extracellular traps sequester circulating tumor cells and promote metastasis. *J. Clin. Invest.* 123:3446–3458. https://doi.org/10.1172/jci67484

Cress, R.D., K. Bauer, C.D. O'Malley, A.R. Kahn, M.J. Schymura, J.M. Wike, S.L. Stewart, and G.S. Leiserowitz. 2011. Surgical staging of early stage epithelial ovarian cancer: results from the CDC-NPCR ovarian patterns of care study. *Gynecol. Oncol.* 121:94–99. https://doi.org/10.1016/j.ygyno.2010.12.359

Daley, J.M., A.A. Thomay, M.D. Connolly, J.S. Reichner, and J.E. Albina. 2008. Use of Ly6G-specific monoclonal antibody to deplete neutrophils in mice. *J. Leukoc. Biol.* 83:64–70. https://doi.org/10.1189/jlb.0407247

Fruhman, G.J. 1960. Neutrophil mobilization into peritoneal fluid. *Blood.* 16:1753–1761.

Fuchs, T.A., U. Abed, C. Goosmann, R. Hurwitz, I. Schulze, V. Wahn, Y. Weinrauch, V. Brinkmann, and A. Zychlinsky. 2007. Novel cell death program leads to neutrophil extracellular traps. *J. Cell Biol.* 176:231–241. https://doi.org/10.1083/jcb.200606027

Fuchs, T.A., A. Brill, D. Duerschmied, D. Schatzberg, M. Monestier, D.D. Myers Jr., S.K. Wrobleski, T.W. Wakefield, J.H. Hartwig, and D.D. Wagner. 2010. Extracellular DNA traps promote thrombosis. *Proc. Natl. Acad. Sci. USA.* 107:15880–15885. https://doi.org/10.1073/pnas.1005743107

Geiser, T., B. Dewald, M.U. Ehrengruber, I. Clark-Lewis, and M. Baggiolini. 1993. The interleukin-8-related chemotactic cytokines GRO alpha, GRO beta, and GRO gamma activate human neutrophil and basophil leukocytes. *J. Biol. Chem.* 268:15419–15424.

Gorelik, E., D.P. Landsittel, A.M. Marrangoni, F. Modugno, L. Velikokhatnaya, M.T. Winans, W.L. Bigbee, R.B. Herberman, and A.E. Lokshin. 2005. Multiplexed immunobead-based cytokine profiling for early detection of ovarian cancer. *Cancer Epidemiol. Biomarkers Prev.* 14:981–987. https://doi.org/10.1158/1055-9965.EPI-04-0404

Granot, Z., E. Henke, E.A. Comen, T.A. King, L. Norton, and R. Benezra. 2011. Tumor entrained neutrophils inhibit seeding in the premetastatic lung. *Cancer Cell.* 20:300–314. https://doi.org/10.1016/j.ccr.2011.08.012

Hagiwara, A., T. Takahashi, K. Sawai, H. Taniguchi, M. Shimotsuma, S. Okano, C. Sakakura, H. Tsujimoto, K. Osaki, S. Sasaki, et al. 1993. Milky spots as

the implantation site for malignant cells in peritoneal dissemination in mice. *Cancer Res.* 53:687–692.

Hakkim, A., B.G. Fürnrohr, K. Amann, B. Laube, U.A. Abed, V. Brinkmann, M. Herrmann, R.E. Voll, and A. Zychlinsky. 2010. Impairment of neutrophil extracellular trap degradation is associated with lupus nephritis. *Proc. Natl. Acad. Sci. USA.* 107:9813–9818. https://doi.org/10.1073/pnas.0909927107

Hashiguchi, Y., M. Kasai, T. Fukuda, T. Ichimura, T. Yasui, and T. Sumi. 2015. Chemotherapy-induced neutropenia and febrile neutropenia in patients with gynecologic malignancy. *Anticancer Drugs.* 26:1054–1060. https://doi.org/10.1097/CAD.0000000000000279

Hemmers, S., J.R. Teijaro, S. Arandjelovic, and K.A. Mowen. 2011. PAD4-mediated neutrophil extracellular trap formation is not required for immunity against influenza infection. *PLoS One.* 6:e22043. https://doi.org/10.1371/journal.pone.0022043

Iwanicki, M.P., R.A. Davidowitz, M.R. Ng, A. Besser, T. Muranen, M. Merritt, G. Danuser, T.A. Ince, and J.S. Brugge. 2011. Ovarian cancer spheroids use myosin-generated force to clear the mesothelium. *Cancer Discov.* 1:144–157. https://doi.org/10.1158/2159-8274.CD-11-0010

Kenny, H.A., T. Krausz, S.D. Yamada, and E. Lengyel. 2007. Use of a novel 3D culture model to elucidate the role of mesothelial cells, fibroblasts and extra-cellular matrices on adhesion and invasion of ovarian cancer cells to the omentum. *Int. J. Cancer.* 121:1463–1472. https://doi.org/10.1002/ijc.22874

Knuckley, B., C.P. Causey, J.E. Jones, M. Bhatia, C.J. Dreyton, T.C. Osborne, H. Takahara, and P.R. Thompson. 2010. Substrate specificity and kinetic studies of PADs 1, 3, and 4 identify potent and selective inhibitors of protein arginine deiminase 3. *Biochemistry.* 49:4852–4863. https://doi.org/10.1021/bi100363t

Ko, S.Y., E. Lengyel, and H. Naora. 2010. The Müllerian HOXA10 gene promotes growth of ovarian surface epithelial cells by stimulating epithelial-stromal interactions. *Mol. Cell. Endocrinol.* 317:112–119. https://doi.org/10.1016/j.mce.2009.12.025

Ko, S.Y., N. Barengo, A. Ladanyi, J.S. Lee, F. Marini, E. Lengyel, and H. Naora. 2012. HOXA9 promotes ovarian cancer growth by stimulating cancer-associated fibroblasts. *J. Clin. Invest.* 122:3603–3617. https://doi.org/10.1172/JCI62229

Ko, S.Y., A. Ladanyi, E. Lengyel, and H. Naora. 2014. Expression of the homeobox gene HOXA9 in ovarian cancer induces peritoneal macrophages to acquire an M2 tumor-promoting phenotype. *Am. J. Pathol.* 184:271–281. https://doi.org/10.1016/j.ajpath.2013.09.017

Kramps, J.A., P. van der Valk, M.M. van der Sandt, J. Lindeman, and C.J. Meijer. 1984. Elastase as a marker for neutrophilic myeloid cells. *J. Histochem. Cytochem.* 32:389–394. https://doi.org/10.1177/32.4.6561228

Lengyel, E. 2010. Ovarian cancer development and metastasis. *Am. J. Pathol.* 177:1053–1064. https://doi.org/10.2353/ajpath.2010.100105

Lewis, H.D., J. Liddle, J.E. Coote, S.J. Atkinson, M.D. Barker, B.D. Bax, K.L. Bicker, R.P. Bingham, M. Campbell, Y.H. Chen, et al. 2015. Inhibition of PAD4 activity is sufficient to disrupt mouse and human NET formation. *Nat. Chem. Biol.* 11:189–191. https://doi.org/10.1038/nchembio.1735

Li, P., M. Li, M.R. Lindberg, M.J. Kennett, N. Xiong, and Y. Wang. 2010. PAD4 is essential for antibacterial innate immunity mediated by neutrophil extracellular traps. *J. Exp. Med.* 207:1853–1862. https://doi.org/10.1084/jem.20100239

Matsui, K., T. Mori, M. Sawada, H. Kuroboshi, H. Tatsumi, T. Yoshioka, M. Akiyama, T. Yamamoto, K. Iwasaku, and J. Kitawaki. 2014. Evaluation of primary prophylaxis with granulocyte colony-stimulating factor for epithelial ovarian cancer. *Eur. J. Gynaecol. Oncol.* 35:48–51.

McDonald, B., R. Urrutia, B.G. Yipp, C.N. Jenne, and P. Kubes. 2012. Intravascular neutrophil extracellular traps capture bacteria from the bloodstream during sepsis. *Cell Host Microbe.* 12:324–333. https://doi.org/10.1016/j.chom.2012.06.011

McNally, L., N.N. Teng, D.S. Kapp, and A. Karam. 2015. Does omentectomy in epithelial ovarian cancer affect survival? An analysis of the Surveillance, Epidemiology, and End Results database. *Int. J. Gynecol. Cancer.* 25:607–615. https://doi.org/10.1097/IGC.0000000000000412

Meng, W., A. Paunel-Görgülü, S. Flohé, A. Hoffmann, I. Witte, C. MacKenzie, S.E. Baldus, J. Windolf, and T.T. Lögters. 2012. Depletion of neutrophil extracellular traps in vivo results in hypersusceptibility to polymicrobial sepsis in mice. *Crit. Care.* 16:R137. https://doi.org/10.1186/cc11442

Metzler, K.D., T.A. Fuchs, W.M. Nauseef, D. Reumaux, J. Roesler, I. Schulze, V. Wahn, V. Papayannopoulos, and A. Zychlinsky. 2011. Myeloperoxidase is required for neutrophil extracellular trap formation: implications for innate immunity. *Blood.* 117:953–959. https://doi.org/10.1182/blood-2010-06-290171

Meza-Perez, S., and T.D. Randall. 2017. Immunological Functions of the Omentum. *Trends Immunol.* 38:526–536. https://doi.org/10.1016/j.it.2017.03.002

Mishalian, I., R. Bayuh, L. Levy, L. Zolotarov, J. Michaeli, and Z.G. Fridlender. 2013. Tumor-associated neutrophils (TAN) develop pro-tumorigenic properties during tumor progression. *Cancer Immunol. Immunother.* 62:1745–1756. https://doi.org/10.1007/s00262-013-1476-9

Mitchell, G.B., B.N. Albright, and J.L. Caswell. 2003. Effect of interleukin-8 and granulocyte colony-stimulating factor on priming and activation of bovine neutrophils. *Infect. Immun.* 71:1643–1649. https://doi.org/10.1128/IAI.71.4.1643-1649.2003

Nathan, C.F. 1989. Respiratory burst in adherent human neutrophils: triggering by colony-stimulating factors CSF-GM and CSF-G. *Blood.* 73:301–306.

Naylor, M.S., G.W. Stamp, W.D. Foulkes, D. Eccles, and F.R. Balkwill. 1993. Tumor necrosis factor and its receptors in human ovarian cancer. Potential role in disease progression. *J. Clin. Invest.* 91:2194–2206. https://doi.org/10.1172/JCI116446

Negus, R.P., G.W. Stamp, M.G. Relf, F. Burke, S.T. Malik, S. Bernasconi, P. Allavena, S. Sozzani, A. Mantovani, and F.R. Balkwill. 1995. The detection and localization of monocyte chemoattractant protein-1 (MCP-1) in human ovarian cancer. *J. Clin. Invest.* 95:2391–2396. https://doi.org/10.1172/JCI117933

Nieman, K.M., H.A. Kenny, C.V. Penicka, A. Ladanyi, R. Buell-Gutbrod, M.R. Zillhardt, I.L. Romero, M.S. Carey, G.B. Mills, G.S. Hotamisligil, et al. 2011. Adipocytes promote ovarian cancer metastasis and provide energy for rapid tumor growth. *Nat. Med.* 17:1498–1503. https://doi.org/10.1038/nm.2492

Park, J., R.W. Wysocki, Z. Amoozgar, L. Maiorino, M.R. Fein, J. Jorns, A.F. Schott, Y. Kinugasa-Katayama, Y. Lee, N.H. Won, et al. 2016. Cancer cells induce metastasis-supporting neutrophil extracellular DNA traps. *Sci. Transl. Med.* 8:361ra138. https://doi.org/10.1126/scitranslmed.aag1711

Passegué, E., E.F. Wagner, and I.L. Weissman. 2004. JunB deficiency leads to a myeloproliferative disorder arising from hematopoietic stem cells. *Cell.* 119:431–443. https://doi.org/10.1016/j.cell.2004.10.010

Pearce, O.M.T., R.M. Delaine-Smith, E. Maniati, S. Nichols, J. Wang, S. Böhm, V. Rajeeve, D. Ullah, P. Chakravarty, R.R. Jones, et al. 2018. Deconstruction of a Metastatic Tumor Microenvironment Reveals a Common Matrix Response in Human Cancers. *Cancer Discov.* 8:304–319. https://doi.org/10.1158/2159-8290.CD-17-0284

Peinado, H., H. Zhang, I.R. Matei, B. Costa-Silva, A. Hoshino, G. Rodrigues, B. Psaila, R.N. Kaplan, J.F. Bromberg, Y. Kang, et al. 2017. Pre-metastatic niches: organ-specific homes for metastases. *Nat. Rev. Cancer.* 17:302–317. https://doi.org/10.1038/nrc.2017.6

Powell, D.R., and A. Huttenlocher. 2016. Neutrophils in the Tumor Microenvironment. *Trends Immunol.* 37:41–52. https://doi.org/10.1016/j.it.2015.11.008

Robinson-Smith, T.M., I. Isaacsohn, C.A. Mercer, M. Zhou, N. Van Rooijen, N. Husseinzadeh, M.M. McFarland-Mancini, and A.F. Drew. 2007. Macrophages mediate inflammation-enhanced metastasis of ovarian tumors in mice. *Cancer Res.* 67:5708–5716. https://doi.org/10.1158/0008-5472.CAN-06-4375

Roby, K.F., C.C. Taylor, J.P. Sweetwood, Y. Cheng, J.L. Pace, O. Tawfik, D.L. Persons, P.G. Smith, and P.F. Terranova. 2000. Development of a syngeneic mouse model for events related to ovarian cancer. *Carcinogenesis.* 21:585–591. https://doi.org/10.1093/carcin/21.4.585

Rollins, B.J., A. Walz, and M. Baggiolini. 1991. Recombinant human MCP-1/JE induces chemotaxis, calcium flux, and the respiratory burst in human monocytes. *Blood.* 78:1112–1116.

Sherman, M.E., P.J. Mink, R. Curtis, T.R. Cote, S. Brooks, P. Hartge, and S. Devesa. 2004. Survival among women with borderline ovarian tumors and ovarian carcinoma: a population-based analysis. *Cancer.* 100:1045–1052. https://doi.org/10.1002/cncr.20080

Sodek, K.L., K.J. Murphy, T.J. Brown, and M.J. Ringuette. 2012. Cell-cell and cell-matrix dynamics in intraperitoneal cancer metastasis. *Cancer Metastasis Rev.* 31:397–414. https://doi.org/10.1007/s10555-012-9351-2

Strobel, T., L. Swanson, and S.A. Cannistra. 1997. In vivo inhibition of CD44 limits intra-abdominal spread of a human ovarian cancer xenograft in nude mice: a novel role for CD44 in the process of peritoneal implantation. *Cancer Res.* 57:1228–1232.

Taki, M., K. Abiko, T. Baba, J. Hamanishi, K. Yamaguchi, R. Murakami, K. Yamanoi, N. Horikawa, Y. Hosoe, E. Nakamura, et al. 2018. Snail promotes ovarian cancer progression by recruiting myeloid-derived suppressor cells via CXCR2 ligand upregulation. *Nat. Commun.* 9:1685. https://doi.org/10.1038/s41467-018-03966-7

Tan, D.S., R. Agarwal, and S.B. Kaye. 2006. Mechanisms of transcoelomic metastasis in ovarian cancer. *Lancet Oncol.* 7:925–934. https://doi.org/10.1016/S1470-2045(06)70939-1

Usui, A., S.Y. Ko, N. Barengo, and H. Naora. 2014. P-cadherin promotes ovarian cancer dissemination through tumor cell aggregation and tumor-peritoneum interactions. *Mol. Cancer Res.* 12:504–513. https://doi.org/10.1158/1541-7786.MCR-13-0489

van Furth, R., J.A. Raeburn, and T.L. van Zwet. 1979. Characteristics of human mononuclear phagocytes. *Blood.* 54:485–500.

Wang, Y., M. Li, S. Stadler, S. Correll, P. Li, D. Wang, R. Hayama, L. Leonelli, H. Han, S.A. Grigoryev, et al. 2009. Histone hypercitrullination mediates chromatin decondensation and neutrophil extracellular trap formation. *J. Cell Biol.* 184:205–213. https://doi.org/10.1083/jcb.200806072

Wculek, S.K., and I. Malanchi. 2015. Neutrophils support lung colonization of metastasis-initiating breast cancer cells. *Nature.* 528:413–417. https://doi.org/10.1038/nature16140

Xu, J., X. Zhang, R. Pelayo, M. Monestier, C.T. Ammollo, F. Semeraro, F.B. Taylor, N.L. Esmon, F. Lupu, and C.T. Esmon. 2009. Extracellular histones are major mediators of death in sepsis. *Nat. Med.* 15:1318–1321. https://doi.org/10.1038/nm.2053

Yokoyama, Y., H. Hirakawa, H. Wang, and H. Mizunuma. 2012. Is omentectomy mandatory in the operation for ovarian cancer? Preliminary results in a rat study. *Eur. J. Obstet. Gynecol. Reprod. Biol.* 164:89–92. https://doi.org/10.1016/j.ejogrb.2012.05.020

Youn, J.I., M. Collazo, I.N. Shalova, S.K. Biswas, and D.I. Gabrilovich. 2012. Characterization of the nature of granulocytic myeloid-derived suppressor cells in tumor-bearing mice. *J. Leukoc. Biol.* 91:167–181. https://doi.org/10.1189/jlb.0311177

Zhang, L., N. Yang, J.R. Garcia, A. Mohamed, F. Benencia, S.C. Rubin, D. Allman, and G. Coukos. 2002. Generation of a syngeneic mouse model to study the effects of vascular endothelial growth factor in ovarian carcinoma. *Am. J. Pathol.* 161:2295–2309. https://doi.org/10.1016/S0002-9440(10)64505-1

Zhou, Q., L. Hong, M.Z. Zuo, and Z. He. 2017. Prognostic significance of neutrophil to lymphocyte ratio in ovarian cancer: evidence from 4,910 patients. *Oncotarget.* 8:68938–68949. https://doi.org/10.18632/oncotarget.20196